*applied sciences*

MDPI

*Article*

# Experimental and Numerical Investigation of Liquid Nitrogen Die Cooling for Increased Efficiency in Porthole Aluminum Extrusion Dies

**Evangelos Giarmas [1,2], Ioannis Theodoridis [2], Panagiotis Tounis [3], Tommaso Pinter [3] and Dimitrios Tzetzis [1,*]**

[1] Digital Manufacturing and Materials Characterisation Laboratory, School of Science and Technology 14th km Thessaloniki-Moudania, International Hellenic University, 57001 Thermi, Greece; egiarmas@gmail.com
[2] Alumil S.A., Production Division, 61100 Kilkis, Greece
[3] Matrex Aluminum Dies S.A., Block 5B-A Road A8 I.A. Sindos, 57022 Thessaloniki, Greece; tommaso.pinter@almax-mori.it (T.P.)
* Correspondence: d.tzetzis@ihu.edu.gr

**Abstract**

Die design plays a critical role in achieving high-quality aluminum extrusion products with optimal efficiency. Porthole dies are widely employed to produce hollow profiles for diverse industrial applications, yet their design parameters significantly influence surface quality, geometry, and productivity. In this study, a two-hole porthole die was investigated using both numerical and experimental approaches. The 6060 aluminum alloy (produced in the foundry of Alumil SA, Kilkis, Greece) was selected as the material of focus. Finite Element Analysis was conducted with HyperXtrude™ 2022 software, while experimental trials were performed on a 35 MN extrusion press. To further enhance productivity, a liquid nitrogen cooling system was integrated into the process. The combined numerical and experimental results demonstrated that the redesigned die and the integration of liquid nitrogen cooling significantly improved process performance. Productivity increased by 8.76%, with ram speed rising from 6.8 mm/s to 9.5 mm/s while maintaining dimensional accuracy and stable extrusion conditions.

**Keywords:** Finite Element Analysis (FEA); aluminum extrusion dies; 6060 aluminum alloy; liquid nitrogen cooling

## 1. Introduction

Finite Element Analysis (FEA) enables optimization of die performance to address key challenges in aluminum extrusion. Porthole extrusion dies are multi-piece tools used to produce hollow aluminum profiles by splitting the billet flow through ports and subsequently welding the streams in a welding chamber. Their design strongly influences metal flow, seam weld quality, and extrusion load. Because of these complexities, understanding and optimizing porthole die behavior is essential for improving product quality and process efficiency. Issues such as surface defects (streaking, spangling), transverse welds, welding surface formation, exit speed variation, and geometry inaccuracies can be minimized using specialized simulation software. FEA also supports material flow optimization, innovative die design evaluation, and productivity-enhancing technologies such as liquid nitrogen cooling [1].

Academic Editor: Valerio Belardi

Received: 13 January 2026
Revised: 19 February 2026
Accepted: 24 February 2026
Published: 28 February 2026

Two main formulations are used to simulate die filling: Arbitrary Lagrangian–Eulerian (ALE) and Eulerian (steady state). ALE incorporates a temperature- and pressure-dependent friction model to capture filling behavior, while Eulerian applies a fixed mesh, limiting filling simulation but reducing computation time. Additionally, Updated Lagrangian analysis models material flow as observed on the press, dividing extrusion into sequential time steps [1]. At each step, nodal velocities update coordinates, while effective strain and other state variables are recalculated. The effective strain $\bar{\boldsymbol{\varepsilon}}$ and other state variables are updated as the following equations indicate [1]:

$$x_{n+1} = x_n + v_{n+1}\Delta t \quad (1)$$

$$\bar{\varepsilon}_{n+1} = \bar{\varepsilon}_n + \acute{\varepsilon}_{n+1}\Delta t \quad (2)$$

where n + 1 and n are the current and previous steps, respectively. Δt is the timestep between them. The main disadvantage to this method is the requirement for repeated remeshing due to large deformation at the entry to the bearing channel.

In Eulerian analysis, the velocity field is computed similarly to the Lagrangian method. This field updates the nodal coordinates of the initially straight extrudate, ensuring the nodes satisfy the governing equation [1]

$$v_f \cdot n = 0 \quad (3)$$

where $v_f$ is the nodal tangential velocity and n is the outward normal from the extrudate surface. The effective strain is based on the following equation [1]:

$$\bar{\varepsilon} = \frac{\partial_{mesh}\,\varepsilon}{\partial t} + v_c \cdot \bar{V}\varepsilon \quad (4)$$

The Arbitrary Lagrangian–Eulerian (ALE) formulation combines the strengths of Eulerian and Updated Lagrangian methods. It employs two mesh systems: the computational reference mesh (CRS) for finite element calculations and the material reference mesh (MRS) that tracks material deformation. Differences between CRS and MRS lead to variables such as effective strain $\bar{\boldsymbol{\varepsilon}}$, defined by the following equation [1]:

$$\frac{\partial_{CRS}\,\bar{\varepsilon}}{\partial t} = \acute{\varepsilon} - (V_{MRS} - V_{CRS}) \cdot \bar{V}\bar{\varepsilon} \quad (5)$$

Bastani et al. [2] carried out a transient simulation of the aluminum extrusion process using the Arbitrary Lagrangian–Eulerian (ALE) algorithm to investigate the influence of process parameters on flow balance and exit temperature. Engelhardt et al. [3] examined the strengths and limitations of Finite Element Analysis (FEA) for predicting material flow and optimizing die design. Their work, using two software solutions based on the discussed formulations, demonstrated accurate flow prediction and reduced tool design time and cost. In another study from Dong et al. [4], an irregular radiator profile was investigated. This research demonstrated how targeted die modifications significantly improve flow uniformity, enabling the extrusion of components that meet the required dimensional and geometric standards. Kloppenborg et al. [5] presented viscoplastic analyses of flow in porthole dies using a modular tool design. Experimental data validated numerical simulations performed with Deform3D and HyperXtrude™. HyperXtrude™ applies an ALE method with a transient moving boundary to capture billet shortening during ram displacement, requiring full process modeling. Deform3D, by contrast, uses a Lagrangian formulation where the mesh follows material flow, necessitating remeshing to maintain quality, because large deformations progressively distort the mesh, degrading element quality and numerical accuracy unless the mesh is periodically regenerated. Components were discretized with linear tetrahedral elements. Results from both codes showed material adhesion to the die walls, while regions away from die edges exhibited constant-velocity flow (Figure 1). Overall, both approaches accurately predicted material flow during

validation. Figure 1 illustrates the predicted flow-line pattern and velocity distribution obtained from both solvers. The flow lines remain nearly parallel and evenly spaced in the central regions, indicating uniform material transport, while their curvature near the die walls reflects the sticking condition and reduced local velocity. The close overlap of the flow-line geometry and the comparable velocity magnitudes between Deform3D and HyperXtrude confirm that both models capture the same deformation pattern and material-flow behavior.

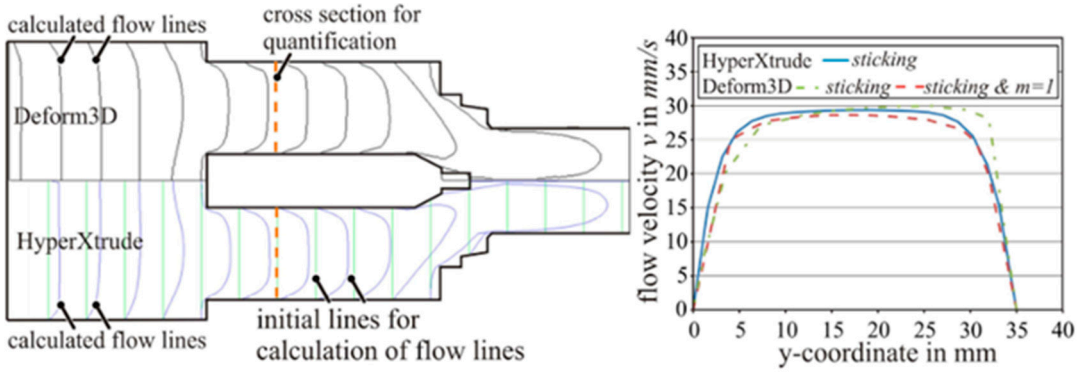


**Figure 1.** Qualitative and quantitative comparison of HyperXtrude™ and Deform3D results.

To address bottom concave defects in extruded hollow aluminum profiles, FEA with HyperXtrude™ 2022 software was employed. Significant velocity and pressure differences were observed between the center and surrounding regions of the section. Introducing baffle plates in the lower part increased central extrusion velocity while reducing external velocity, lowering maximum Y-direction displacement at the profile base from 1.1 to 0.15 mm and markedly improving concave defects [6].

Chen et al. [7] conducted a Finite Element Analysis of the extrusion process for a large hollow profile. To achieve more uniform velocity and temperature distributions in the extrudate, they modified the porthole die by reducing the porthole area, incorporating a baffle plate, and adjusting the bearing length. Zhang et al. [8] investigated extrusion of a complex thin-walled aluminum profile for high-speed trains, demonstrating that modifying baffle plate layout, shape, and height achieved dimensionally accurate sections. Their results highlighted the critical role of baffle plates in balancing material flow, with the Velocity Relative Difference reduced by 84.5% to 6.3% in the optimized design. Numerical analysis confirmed die stress and deflection remained within allowable limits, while experimental validation on an 80 MN press produced sections with a rib thickness deviation of only 0.12 mm and no heat defects, confirming the effectiveness of the die modification process.

Truong et al. [9] designed a die for extrusion of a complex heatsink aluminum profile with variable wall thickness, combining experimental design techniques with steady-state ALE simulation. Modifications to porthole and pocket structures, port bridge design, and bearing lengths improved flow balance. Compared to the initial die, velocity distribution measures (ΔV and VRD) decreased from 4.72 mm/s and 4.1% to 0.86 mm/s and 0.82%. Residual stresses and extrusion force were reduced from 16.19 MPa and 479.55 tons to 12.83 MPa and 477.88 tons, while peak exit temperature rose slightly. These results confirmed the effectiveness of the optimized die design.

$$\Delta V = V_{max} - V_{min} \quad (6)$$

$$VRD = \frac{\sum_{i=1}^{n} \frac{|vi - va|}{va}}{n} \times 100\% \quad (7)$$

where $v_i$ is the extrusion velocity for node i on the extruded section, $v_a$ is the average velocity calculated from the total number of nodes of the extrudate and n is the number of nodes considered in a cross-section of the extruded section.

Peng and Sheppard [10] investigated the pocket's influence on material flow in multi-hole extrusion using three-dimensional FEA. They examined temperature variation, exit velocity, and deformation history across the die orifice, with experimental validation confirming accuracy. The results showed that proper pocket design ensures uniform flow, while even small offsets significantly alter material behavior. Poorly designed pockets led to deterioration in temperature, velocity, and structural uniformity at the surface.

Sun et al. [11] investigated the use of a second-step chamber in extrusion dies for condenser tube aluminum alloy profiles. Their study demonstrated that this design achieved a uniform velocity distribution across the section and improved die strength. Adoption of the second-step chamber proved especially beneficial for complex multicavity dies, reducing the Standard Deviation of the Velocity field (SDV) from 4.37 mm/s in the initial design to 0.29 mm/s in the optimized one, a 93.36% improvement. The SDV is defined as follows:

$$\text{SDV} = \sqrt{\sum_{i=1}^{n} \frac{(v_i - \bar{v})\text{^}2}{n}} \quad (8)$$

where $v_i$ is the extrudate velocity of node i in the cross-section to be researched, $\bar{\mathbf{v}}$ is the average axial velocity for the selected nodes and n is the number the nodes in total. Finally, the strength of the optimal designed dies was also verified and the die maximum stress was calculated at 430 MPa, much less than the yield stress of H13 steel (1.180 MPa).

Growing industrial interest now centers on reducing scrap from front-end defects such as charge welds and back-end defects like billet skin contamination, both critical for improving product quality and process efficiency. Regarding charge weld extent estimation, a novel analytical approach was recently proposed [12].

$$d = E_f \cdot C_f \cdot \frac{V}{A_e \cdot n} \quad (9)$$

$$E_f = \frac{A_{Pmax}}{A_{Pavg}} \quad (10)$$

where the charge weld extent (d) has been connected to the volume of material in the die (V); to an extrusion factor (Equation (10)), where $A_{pmax}$ is the cross-sectional area of the biggest port and $A_{pavg}$ is the average cross-sectional area of the ports; to the exit profile section area (Ae); and to the number of profile holes in the die (n). The corrective factor $\mathbf{C_f}$ is not constant, as previously proposed [13,14], but varies depending on die design. Jowett et al. [14] proposed an equation for skin contamination as well.

$$\text{s} = \frac{(14\%\ x\ Vb - 75\ x\ (V1+V2) - V_{butt})}{Ae\ x\ n} \quad (11)$$

where $V_{butt}$ and $V_b$ are the butt end and billet volume, respectively; V1 is the volume of material in the die ports; V2 is the volume of material in the welding chambers; and the other terms follow the definitions used in previous equations.

Zhang et al. [15] developed an optimization system to improve porthole structures in extrusion dies, creating automatic software based on the Finite Volume Method (FVM) with non-orthogonal Euler grids. Since aluminum alloys at high temperature behave as non-Newtonian fluids, several researchers, including Wu et al. [16], Gonçalves et al. [17], and Basic et al. [18], applied FVM to extrusion simulations, producing algorithms capable of handling unstructured meshes for complex die designs. Zhang et al. [14] focused on a multi-hole tube extrusion die, using their software to refine porthole geometry. Compared to the initial die, the optimized design achieved a more uniform velocity distribution and reduced corner deformation, with the velocity difference and Standard Deviation of

Velocity (SDV) lowered by 55% and 69%, respectively. Subsequent comparison with HyperXtrude™ confirmed that velocity distribution trends and values closely matched, validating the new optimization tool.

Mahmoodkhani et al. [19] examined the influence of feeder geometry, comparing a regular round pocket with a tapered design. Finite Element Analysis using Deform™ software was validated against experimental data, revealing significant effects on dead metal zone size and the thickness and length of transverse welds in extruded sections. The tapered feeder facilitated depletion of residual billet material, thereby reducing dead zones and weld formation compared to the round pocket. Predicted extrusion load and exit temperature, however, remained largely unaffected by the geometry change. Figure 2 illustrates the two feeder configurations.

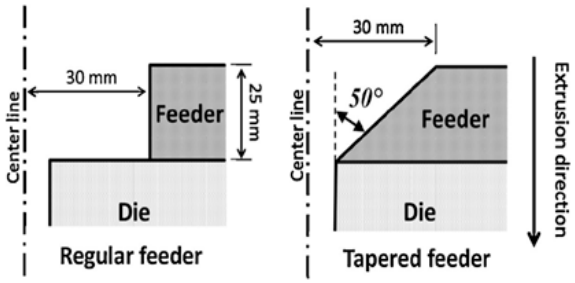


**Figure 2.** Regular and tapered feeder geometry.

Simulation results indicated that extrusion ratio strongly influences transverse weld length, which increases as the ratio rises. Yu et al. [20] reported that the depth of the welding chamber significantly affected the evolution of transverse seams, while its impact on seam length was relatively minor. Reggiani et al. [21] compared experimental and numerical approaches for predicting charge weld formation, showing that empirical rules based solely on extrusion ratio produced large errors, up to 42.9%, and were therefore unreliable. Corrected analytical formulas yielded average errors of 4% compared to 31.6% for uncorrected ones, while numerical predictions showed higher deviations. Analytical models corrected with a factor of 1.5 achieved a lower mean error but greater variability, whereas Finite Element Analysis produced a slightly higher average error but more consistent results. FEA was validated as a powerful tool for predicting charge weld formation, though computational time varied widely with die and profile complexity, ranging from 10 to 132 h. This study concluded that more advanced analytical formulations incorporating additional die design factors and extrusion parameters are needed for accurate weld length prediction.

Monitoring extrusion temperature is essential for extending die life, preventing defects, and improving productivity in aluminum alloy processing. Several methods exist to control exit temperature, including tapered billets and reduced preheating, though these offer limited productivity gains and increase die failure risk [22,23]. Isothermal extrusion, which regulates exit temperature through closed-loop ram speed control, has also been applied [24]. More recently, rising demand for high-quality extrudates at competitive prices has highlighted liquid nitrogen cooling as a promising solution [25–27]. While effective in removing heat from dies, its success depends heavily on careful design of cooling channels, including their shape, depth, and placement of inlets and outlets.

Recent research has shown a renewed industrial and scientific interest in liquid-nitrogen cooling as an effective strategy to enhance aluminum extrusion performance. $LN_2$ cooling is now widely adopted to reduce profile exit temperatures, improve surface quality, and enable higher ram speeds, yet the design of cooling channels in industrial practice still relies heavily on empirical, experience-based approaches that often lead to

suboptimal thermal management. Several studies have demonstrated that trial-and-error design is both time-consuming and costly, motivating the development of reliable numerical tools capable of predicting and optimizing nitrogen-assisted cooling during die design. Experimental campaigns on AA6060 profiles, combined with fast numerical models in COMSOL Version 6.1 Multiphysics, have shown good agreement between simulated and measured die temperatures, extrusion loads, and cooling efficiency, revealing how far conventional cooling-channel layouts are from optimal configurations. Complementary investigations have also examined the mechanical implications of $LN_2$-enabled higher ram speeds, showing that while tensile strength remains largely unaffected, elongation and creep behavior exhibit measurable sensitivity to the enhanced thermal conditions. Together, these recent contributions highlight the growing importance of advanced, simulation-driven cryogenic cooling strategies and reinforce the need for improved modelling approaches to support modern extrusion practice [28–30]. Design guidelines emphasize simplicity, since multiphase flow calculations are complex and friction effects reduce accuracy. Manufacturers therefore adopt straightforward rules that allow economical construction of cooling channels in backers. Figure 3 illustrates nitrogen channel arrangements developed during die design studies, showing both the installed factory system and the principles for achieving uniform cooling. In practice, liquid or gaseous nitrogen enters through the supply region, passes into the distributor ring, and is directed by feeders into cooling channels before reaching the injectors and extrudate. Channel layout reflects profile symmetry, hole number, and backer constraints, though further reworking after initial trials is often impractical.

Although many studies have examined aluminum extrusion, research on porthole dies often relies mainly on simulations, with limited validation under industrial conditions. The combined effects of die redesign and advanced cooling strategies also remain insufficiently explored, and existing works rarely provide clear metrics for evaluating productivity. These gaps motivate the present study, which investigates a redesigned two-hole porthole die for AA6060 with the aim of increasing extrusion productivity while maintaining stable process conditions. The novelty lies in integrating Finite Element Analysis with full-scale extrusion trials, incorporating liquid-nitrogen cooling, and introducing a new approach for assessing extrusion efficiency. To achieve this, HyperXtrude™ simulations were performed and validated through experiments on a 35 MN press.

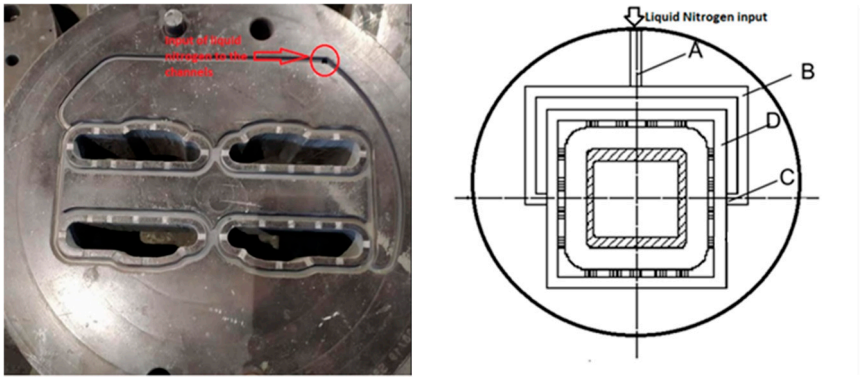


(**a**) (**b**)

**Figure 3.** (**a**) Liquid nitrogen channels. The red arrow indicates the liquid nitrogen input. (**b**) Graphical representation of cooling channels. The liquid/gaseous nitrogen has its source in supply region A and comes into the outer ring or distributor B. After that the feeder C leads the nitrogen to the cooling channels D. Red arrow indicates the input of liquid nitrogen to the channels.

## 2. Experimental Details and Computational Methodology

### *2.1. Experimental Details*

The methodology adopted in this research is presented below. The experimental phase was carried out on a 35 MN direct-extrusion press, where the process parameters were systematically monitored to identify opportunities for die-design optimization. The trials were performed using AA6060 billets (produced in the foundry of Alumil SA, Kilkis, Greece) at industrially relevant temperatures, with controlled variations in ram speed, die temperature, and the application of liquid nitrogen cooling. Each billet was extruded under steady-state conditions, and real-time production data—including ram pressure, exit temperature, and profile geometry—were recorded for subsequent comparison with the numerical predictions. The overall workflow, including the evaluation of the initial die, the optimization through FEA, and the final validation with the manufactured optimized die, is illustrated in Figure 4. A specific industrial profile and its corresponding porthole die were selected as the case study for this investigation. In addition to structural die optimization, the study also investigates the use of liquid nitrogen cooling as a complementary enhancement technique. $LN_2$ cooling is introduced here as an additional optimization strategy aimed at improving thermal stability and enabling higher ram speeds in industrial extrusion conditions.

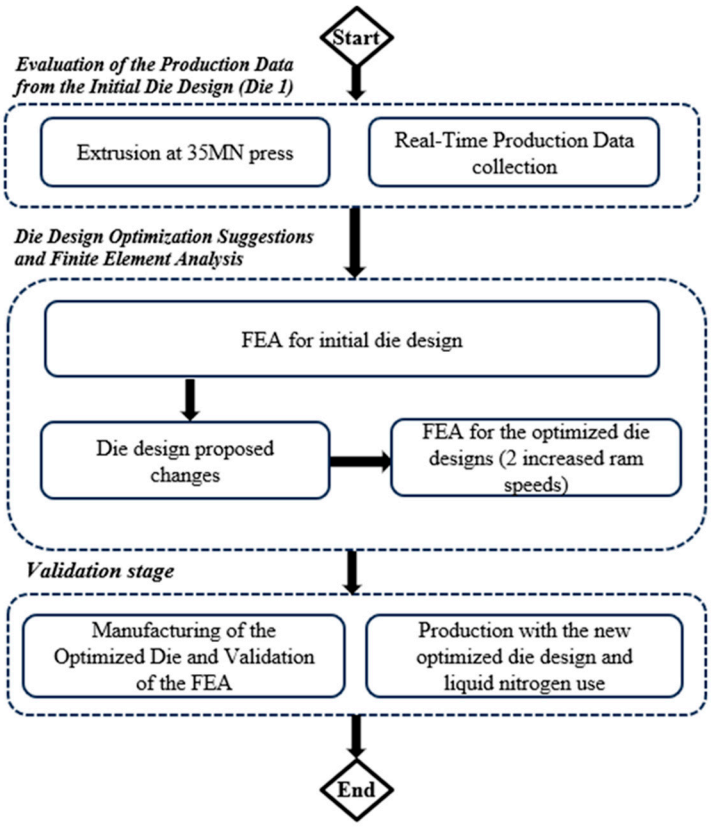


**Figure 4.** Flowchart of the current research.

Regarding the extrusion ratio of the selected extrudate, it is important to stress its significance in aluminum extrusion. The extrusion ratio is a key parameter that indicates the extent of deformation the material undergoes. It is defined as the ratio between the billet's cross-sectional area and the cross-sectional area of the final extruded profile. A higher extrusion ratio signifies greater material reduction, typically resulting in improved surface finish and enhanced mechanical properties due to increased plastic deformation. However, it also demands higher extrusion forces and accelerates die wear. Conversely,

lower extrusion ratios require less force and are better suited for complex or hollow profiles, though they may not provide the same level of surface refinement. Selecting an appropriate extrusion ratio is therefore essential for achieving a balance between productivity, material behavior, and die longevity in industrial applications.

This study also evaluated a redesigned die that employs liquid nitrogen as a cooling medium. The main goal was to enhance productivity by enabling higher ram speeds while maintaining excellent geometric and surface quality. Liquid nitrogen cooling helps keep temperatures near the bearings within acceptable limits, thereby reducing adverse effects on the extrudate surfaces.

### 2.2. Computational Methodology

The proposed die design modifications were analyzed using FEA with HyperXtrude™ software. This simulation offered detailed insights into how the modifications influenced die performance. Based on the FEA outcomes, the most suitable modifications were finalized in the later stages of the optimization process.

To explore potential corrective actions for the extrudate produced with Die 1, simulations of the original die design were carried out using HyperXtrude™ 2022 software. HyperXtrude™ 2022, which employs the Arbitrary Lagrangian–Eulerian (ALE) method, cannot simulate the die filling phase but offers advantages such as reduced computational time. The software is primarily optimized for steady-state analysis and therefore cannot fully resolve the transient die-filling phase, during which the material front advances and the flow field evolves rapidly. As a result, HyperXtrude™ 2022 assumes that the material flow has already reached a fully developed state at the die entrance and within the bearing regions. This simplification affects the accuracy of predictions related to initial flow imbalances, transient dead-metal zone formation, and early-stage surface defect development. Despite these limitations, the tool remains highly effective for evaluating steady-state stress distributions, temperature fields, and material flow patterns, which are the focus of the simulations presented in this work. Furthermore, thermal boundary conditions were defined by heating the billet to 470 °C, maintaining the die at 500 °C, and setting the container temperature to 430 °C, creating realistic thermal gradients during extrusion. The billet length was set to 1000 mm, and a ram speed of 6.7 mm/s was used to replicate actual production conditions. Together, these parameters formed a high-fidelity model capable of accurately predicting material flow, temperature distribution, and stress concentrations within the die. Mesh convergence analysis has also been carried out in order to ensure the validity of the outcomes. Three mesh levels were examined: a coarse mesh, a medium mesh, and the final fine mesh consisting of 3.8 M elements and 870k nodes. The comparison focused on the predicted material velocity at the die exit, which is a sensitive indicator of flow balance in extrusion. As the mesh was refined, the exit-velocity predictions progressively stabilized, and the difference between the medium and fine meshes became very small (on the order of 1–2%), indicating that further refinement did not meaningfully alter the solution. This confirms that the adopted fine mesh provides mesh-independent predictions for both the flow field and the stress distribution. In more detail, a quantitative convergence criterion was applied. The refinement was continued until the change in predicted exit velocity between successive mesh levels fell below 2%, a commonly accepted threshold for extrusion-flow simulations. The difference between the medium and fine meshes was within 1–2%, and no further changes were observed, indicating that the adopted fine mesh provides mesh-independent predictions.

The thermophysical properties of AA6060 were implemented in HyperXtrude™ 2022to ensure consistent thermo-mechanical coupling. The alloy density was set to 2700 kg/m$^3$, with a specific heat capacity of about 900 J/kg·K and a thermal conductivity of 210 W/m·K.

Symmetry boundary conditions (SymmetryBC) were applied along the planes of symmetry, allowing only half of the geometry to be modeled. Thermal interaction at the tool–billet interface was captured using a convective heat transfer coefficient of 3000 W/m²°C, the default value in HyperXtrude™ 2022. This value reflects the strong thermal coupling between the hot billet and the steel tooling during steady-state extrusion. Although the heat-transfer coefficient can influence numerical convergence and temperature predictions, preliminary sensitivity checks showed that the default value provided stable solutions and temperature levels consistent with typical industrial extrusion conditions. For this reason, and to maintain compatibility with established HyperXtrude™ 2022 modeling practices, the value of 3000 W/m²°C was adopted in the present simulations. All extrusion trials were simulated under full-stick friction conditions in both the main die body and the bearing region, in accordance with Hoque et al. [31]. According to this study, several friction models were tested, but all options other than the full-stick boundary condition significantly underestimated the extrusion force and exhibited convergence difficulties, particularly at higher ram speeds and under $LN_2$ cooling. To refine the analysis, Stick boundary conditions were applied to the SolidWall regions (billet surface and pocket–die interface), while the friction coefficient in the bearing region was varied from the default value of 0.3 up to 1.0. The simulations showed that only the full-stick condition reproduced the experimentally measured extrusion load with acceptable accuracy. For this reason, full-stick friction was adopted in both the SolidWall and bearing regions for all simulations, ensuring numerical stability and consistency with the experimental observations.

Following the simulation phase, the dies were manufactured and tested experimentally on the 35 MN extrusion press. These trials aimed to confirm whether the new die design and liquid nitrogen cooling successfully delivered the targeted increase in productivity. At the same time, the extrudates were evaluated for geometric accuracy and surface finish to ensure compliance with quality standards.

The simulation outcomes were validated through a thorough comparison with experimental data. This verification step ensured that the FEA reliably predicted die performance on an industrial scale. Validation included a detailed assessment of the extrudates produced during the experimental trials.

A distinguishing element of this research is the development of a new method (Equation (12)) for evaluating extrusion process efficiency. Traditional industrial metrics, such as set point or average ram speed, proved inadequate for this purpose. The proposed efficiency equation calculates the ratio of the theoretical time required to extrude a specific length and number of billets to the actual time achieved. When the actual time is shorter than the theoretical time, the efficiency surpasses 100%, marking a new performance benchmark. This equation is expected to support industry efforts toward improved efficiency, higher product quality, and more sustainable, cost-effective manufacturing.

The theoretical extrusion time is determined using a standardized ram speed, accounting for billet length, the selected ramp speeds at the start and end of extrusion, the dead time between billets, and the total number of billets. Billet length is particularly influential, as longer billets yield longer extruded sections, higher productivity, and reduced scrap. Consequently, when extrusion efficiency is low, parameters such as billet length, ram speed, billet temperature, and die design should be examined to identify opportunities for improvement. The sum of these calculations provides the theoretical extrusion time. This equation is vital because it evaluates production efficiency not only through ram speed but by incorporating all significant extrusion parameters.

The theoretical extrusion time represents the minimum achievable production time for a given die and alloy under ideal but realistic operating conditions. It is calculated by assuming that the press operates continuously at the maximum stable ram speed recorded

during the run, while still accounting for all unavoidable process interruptions. Specifically, the theoretical time is defined as the sum of four components: (i) the extrusion time at maximum ram speed, obtained by dividing the billet length by the maximum stable speed; (ii) the ramp-up time required at the beginning of each billet to accelerate from the initial speed to the maximum speed; (iii) the controlled slowdown time applied at the end of each billet to ensure a smooth tail-out; and (iv) the billet-change dead time between successive billets. By combining these elements, the theoretical time reflects the fastest possible cycle that could be achieved under the same operational constraints, thereby providing a meaningful baseline against which the real extrusion time can be compared.

Moreover, concerning the methodological contribution of this metric, it is important to note that it does more than restate a time ratio, as it formalizes, for the first time, a unified framework that integrates all major extrusion-cycle components (ram acceleration, steady-state deformation speed, controlled deceleration, and billet-change dead time) into a single, comparable efficiency indicator. Unlike traditional metrics based solely on set-point or average ram speed, the proposed formulation explicitly incorporates the maximum stable ram speed as a process-specific limit derived from real operating data. Although the value of the maximum stable ram speed influences the theoretical extrusion time, reasonable variations in this parameter have only a limited effect on the resulting efficiency because the metric is governed not solely by steady-state speed but by the combined contributions of ramp-up, slowdown, and billet-change intervals. This demonstrates that the metric is robust to reasonable uncertainty in speed selection and remains applicable across different dies, alloys, and operating strategies. By quantifying the gap between theoretically achievable and actual cycle times, the metric provides a process-agnostic baseline that can be used to compare performance across shifts, presses, or die designs, thereby establishing its value as a methodological tool rather than a simple reformulation of existing time-based indicators.

$$\text{Efficiency (\%)} = \frac{\text{Theoretical extrusion time in hours}}{\text{Real extrusion time in hours}} \quad (12)$$

where

$T_{theoretical} = T_{extrusion\ at\ max\ speed} + T_{ramp} + T_{slowdown} + T_{billet\text{-}change}$:

- $T_{extrusion\ at\ max\ speed}$ = billet length/maximum recorded ram speed;
- $T_{ramp}$ = time required to accelerate from initial speed to maximum speed;
- $T_{slowdown}$ = controlled deceleration time at the end of each billet;
- $T_{billet\text{-}change}$ = dead time between billets.

### *2.3. Evaluation of the Production Data from the Initial Die Designs*

In this study, the chosen extrudate is referred to as Die 1, as shown in Figure 5. The target dimensions are shown in Figure 5, and the objective of this work was to enhance the overall productivity of the die while maintaining the dimensions within the specified tolerances.

The technical drawing of the above die is presented below. The extrusion ratio for the above profile is ERcode1 = 70.16. The initial die design for the above design had two holes. The initial die design is also shown in Figure 6.

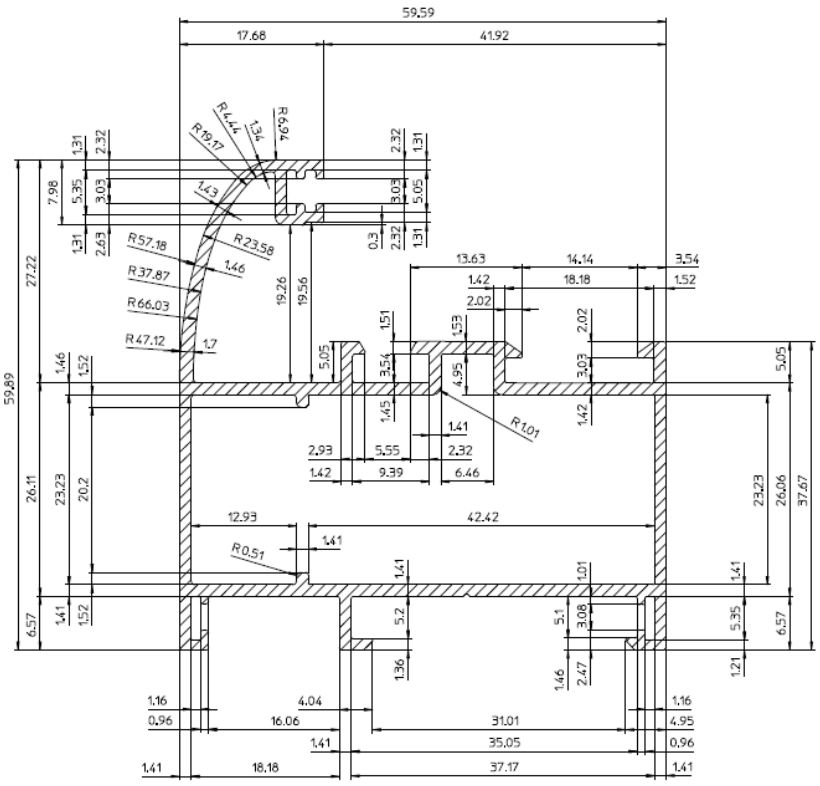


**Figure 5.** Geometry of extrudates with Die 1.

Production trials for the previously described die were carried out on the 35 MN press. The outcomes of these trials, along with the corresponding extrusion parameters, are summarized in Table 1. The temperatures of the first three zones in the preheating furnaces are also included in the table, and these zones are clearly illustrated in Figure 7. All temperature values were recorded directly from the extrusion press's SCADA system, with real-time data captured by thermocouples installed inside the furnace. Efficiency was determined by calculating the ratio between the theoretical time needed to extrude a specified number of billets and the actual time recorded during the production trial. A higher ratio signifies improved productivity. As shown in Figures 8 and 9, the maximum ram speed reached 6.8 mm/s, while the maximum pressure in the main cylinder ranged between 240 and 250 bar.

**Table 1.** Production data for initial die design for extrudate with Die 1.

| Profile Code | Billet Length (mm) | Temp. at Zone 1 (°C) | Temp. at Zone 2 (°C) | Temp. at Zone 3 (°C) | Efficiency |
|---|---|---|---|---|---|
| 1 | 1000 | 470 | 450 | 430 | 84.50% |

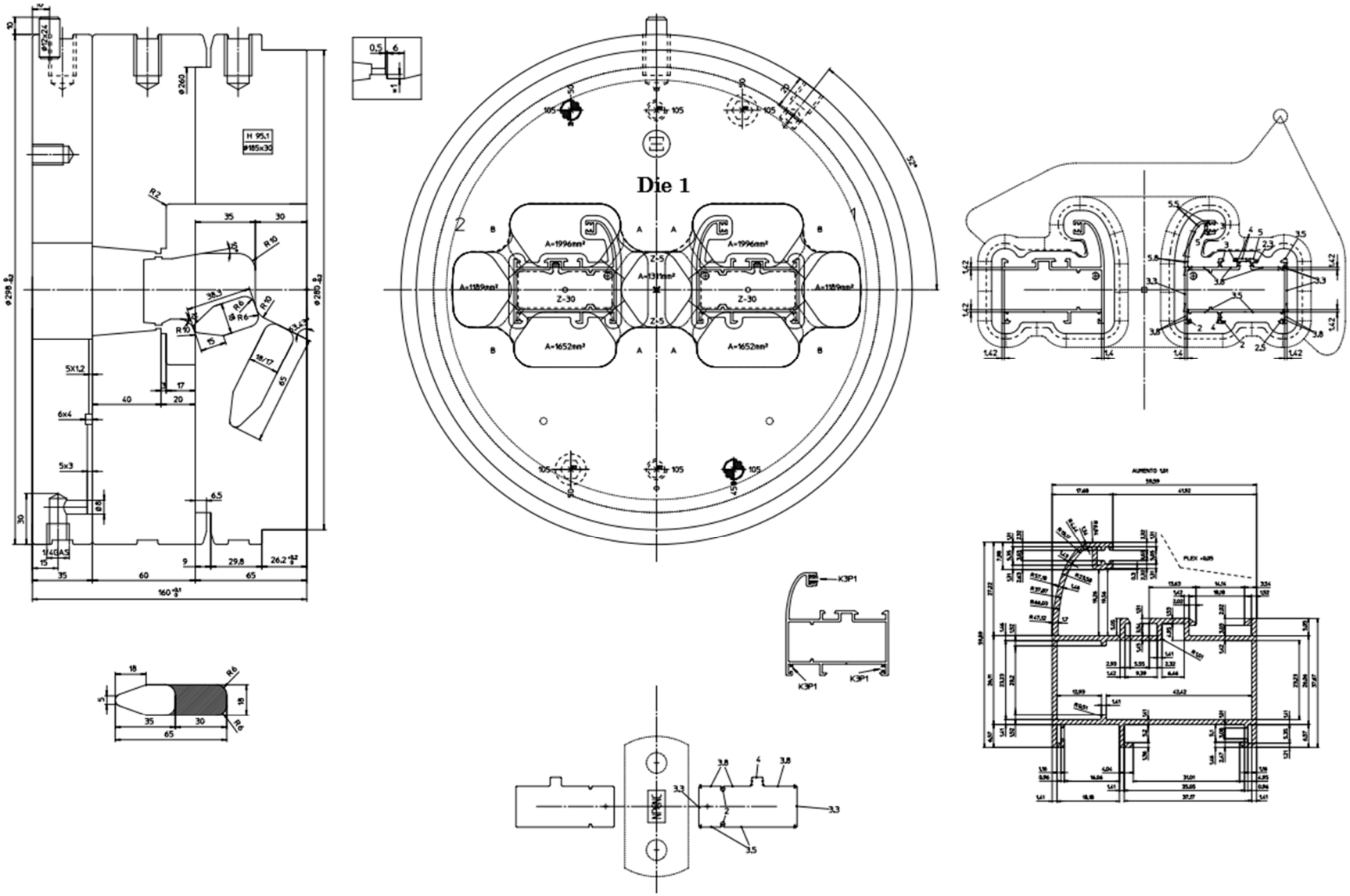


**Figure 6.** Technical drawing for the initial die design of extrudate with Die 1.

https://doi.org/10.3390/app16052385


**Figure 7.** The first 3 preheating zones in the billet oven.

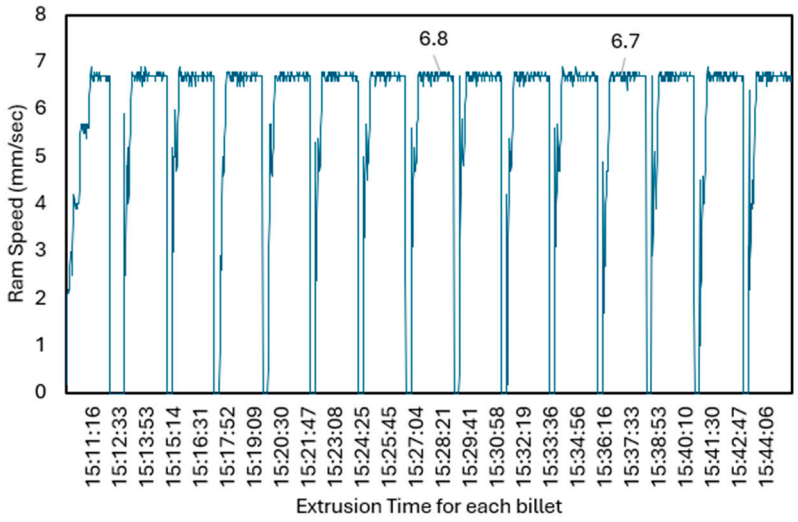


**Figure 8.** Ram speed for initial die design for extrudate with Die 1.

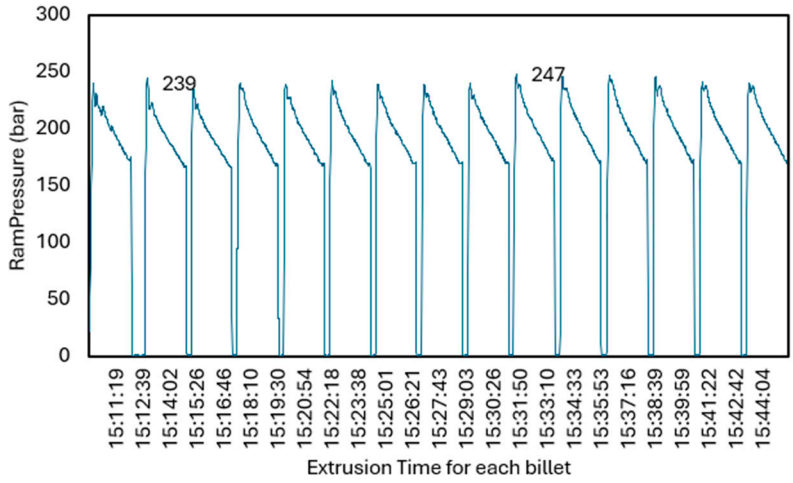


**Figure 9.** Ram pressure for initial die design for extrudate with Die 1.

## 3. Results and Discussion

### *3.1. Die Design Finite Element Analysis Optimization*

The die design optimization process focused on achieving higher efficiency while preserving the geometric accuracy and surface quality of the extruded products. The initial die design approach was first evaluated using FEA, after which the proposed modifications were implemented. Finite element models were then developed, and simulations were performed to assess how these modifications influenced the extrudate. For the optimized die configuration, two different ram speeds were selected to evaluate die performance at elevated extrusion rates, enabled by the use of liquid nitrogen cooling.

The FEA (HyperXtrude™ 2022 software) of the aluminum extrusion die for Profile Die 1 used a detailed mesh consisting of 871,523 nodes and 3,818,714 elements. Tetrahedral elements were assigned to both the aluminum billet and the die plates, while the extruded profile was modeled with prismatic elements to better represent its geometry. Details of the analysis and the corresponding FEA model are shown in Figure 10.

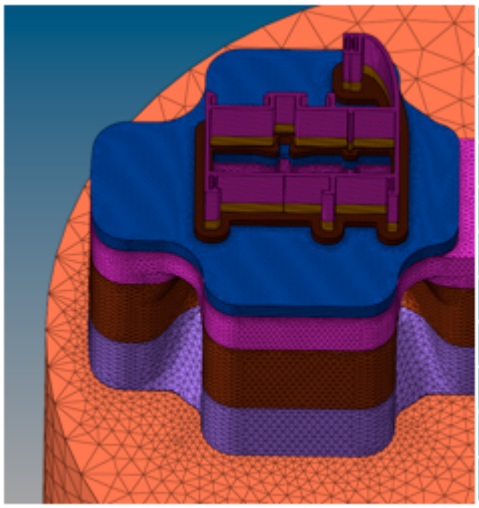

| Profile Code | 1 |
|---|---|
| N° of nodes | 871,523 |
| N° of elements | 3,818,714 |
| Mesh type Aluminium | Thetraedric |
| Mesh type Profile | Prismatic |
| Mesh type Plates | Thetraedric |
| Billet Temperature (°C) | 470 |
| Billet Length (mm) | 1000 |
| Die Temperature (°C) | 500 |
| Container Temperature(°C) | 430 |
| Ram Speed (mm/sec) | 6.7 |

**Figure 10.** FEA model and simulation details for initial die design of Die 1. The different colors in the mesh represent distinct flow-domain regions, corresponding to the progressive stages of the material as it enters and advances through the die entry zones.

### *3.2. Initial Die Design Simulation Results*

Figures 11–15 present the simulation results for the initial die design, referred to as Die 1. Figure 15 also provides a graphical representation of the direction of the extruded sections after exiting the press. A detailed review of Figure 11 shows a substantial deviation in the average exit speed. It should be emphasized that the velocity variations at the upper part of the curved section in the extrudate were not taken into account, as these speeds must intentionally be increased to achieve the correct final dimensions. This area will therefore be deliberately adjusted in the optimized die design. For the remaining portions of the profile, the difference between the maximum and minimum relative exit speeds was found to be 52%.

Furthermore, as illustrated in Figure 12, the tendency of the extrudate to shift toward the bottom center of the die requires improvement. As the profile exits the press, the lower exit speeds observed in the bottom and lateral regions cause the material flow to drift downward and inward. With the introduction of liquid nitrogen cooling and the corresponding increase in ram speed, these tendencies are expected to become even more pronounced, potentially creating significant challenges during extrusion.

Regarding the temperatures at the bearings, Figure 13 indicates that there are no substantial deviations likely to cause surface defects on the extrudate. Additionally, the mandrel displacement in the Y-axis, shown in Figure 14, is predicted to shift downward by approximately 0.02 mm. Figure 15 further shows that the displacement of the mandrels in the Z-axis is estimated at 0.28 mm. Taken together, particularly the large exit speed variation, these results highlight the need for a more refined die design to address the identified issues and to support optimization for higher productivity.

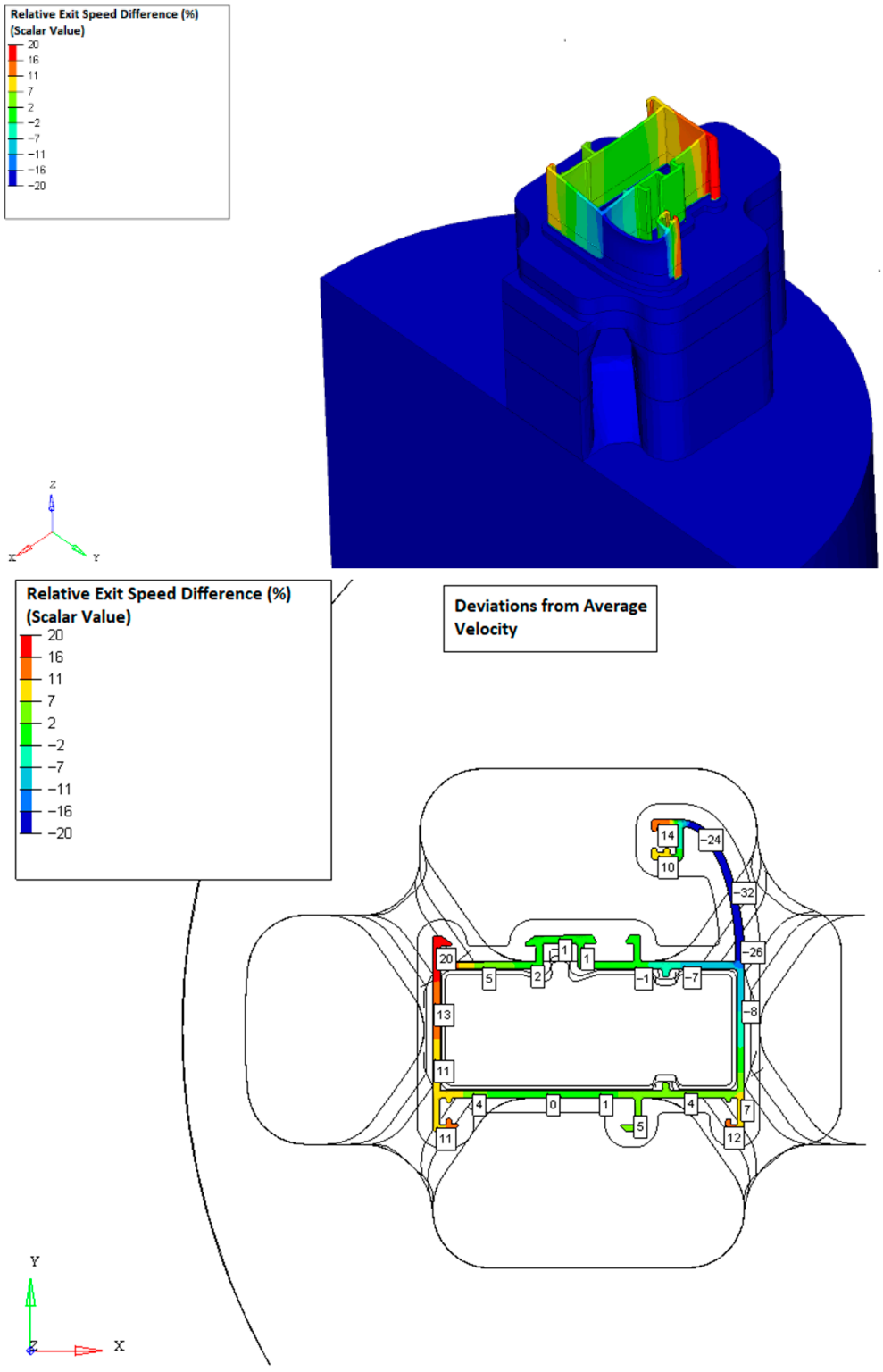


**Figure 11.** Relative exit speed difference for the initial die design of Die 1.

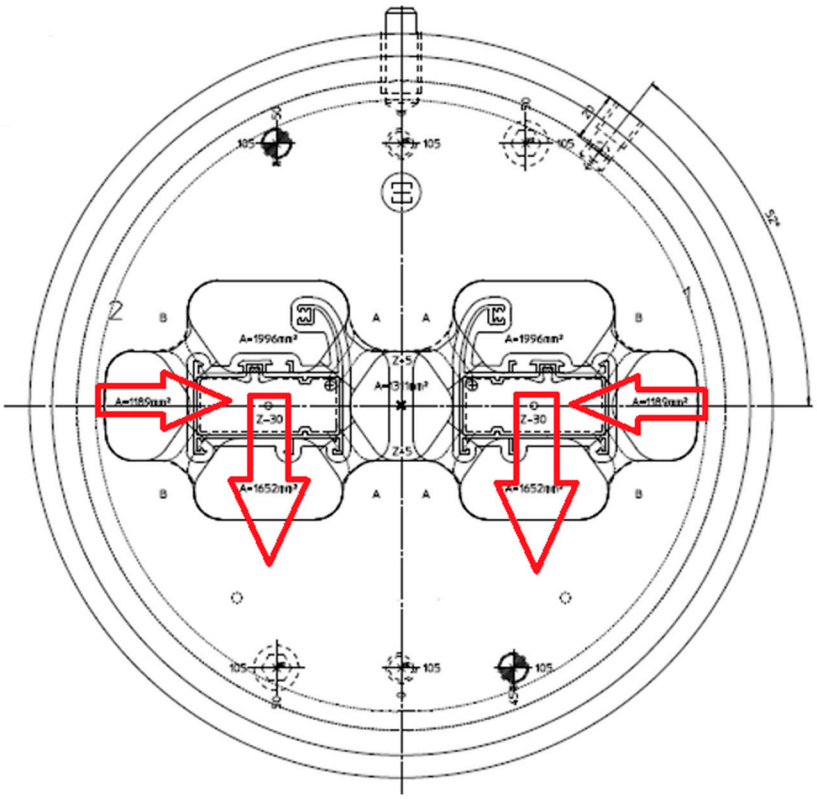

**Figure 12.** Extruded sections' direction for the initial die design of Die 1. The red arrows indicate the direction of the profiles as soon as they exit the die.

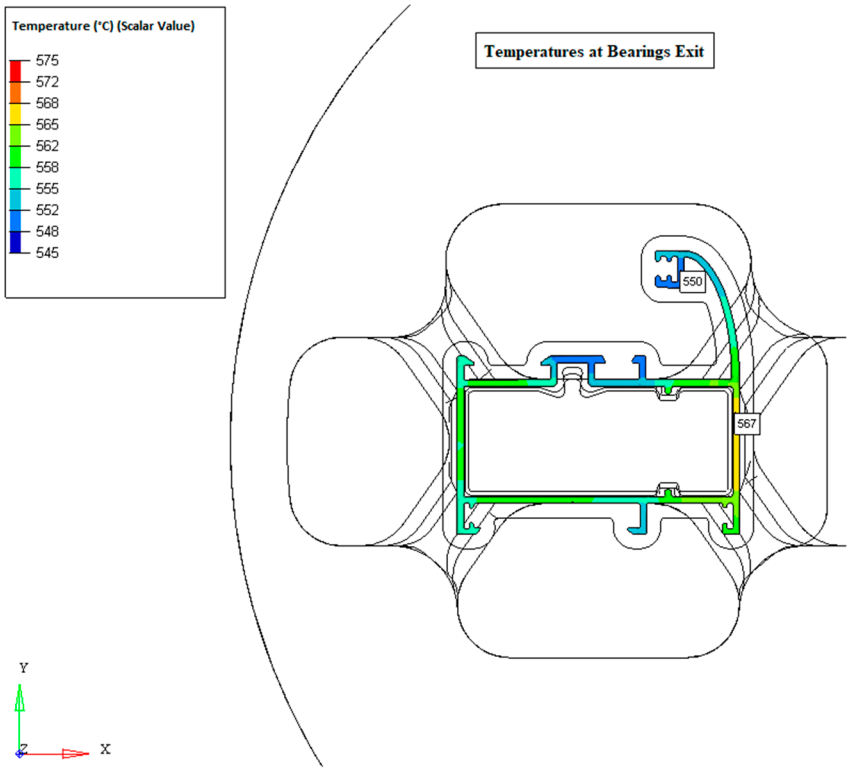


**Figure 13.** Temperatures at bearing exit for the initial die design of Die 1.

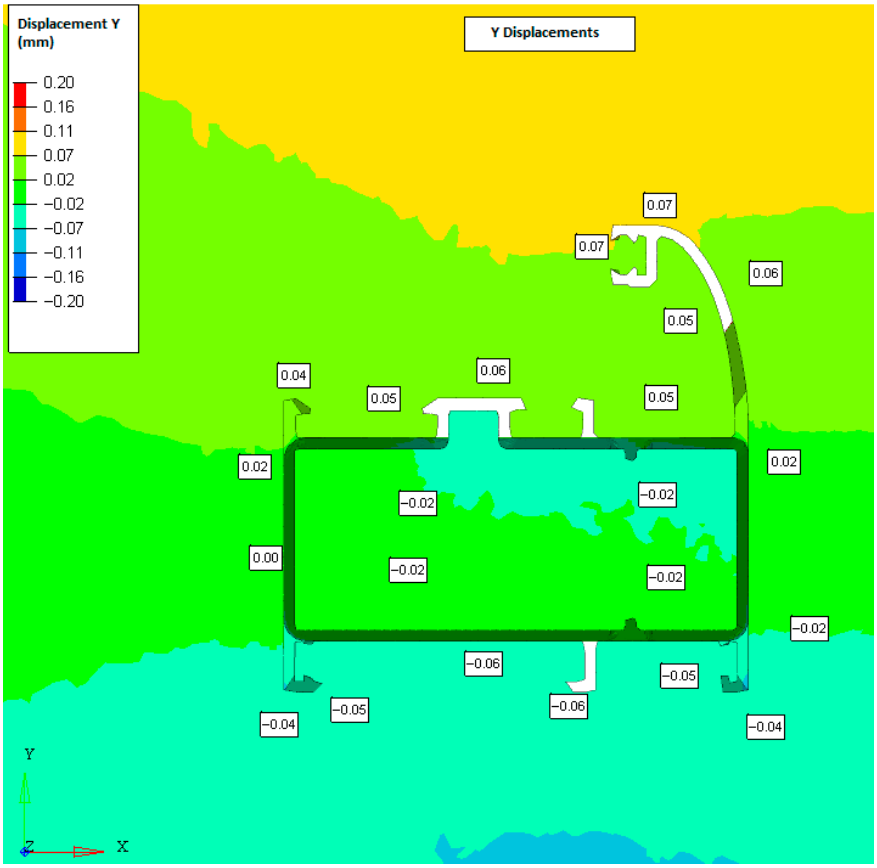


**Figure 14.** Displacement (Y) for the initial die design of Die 1.

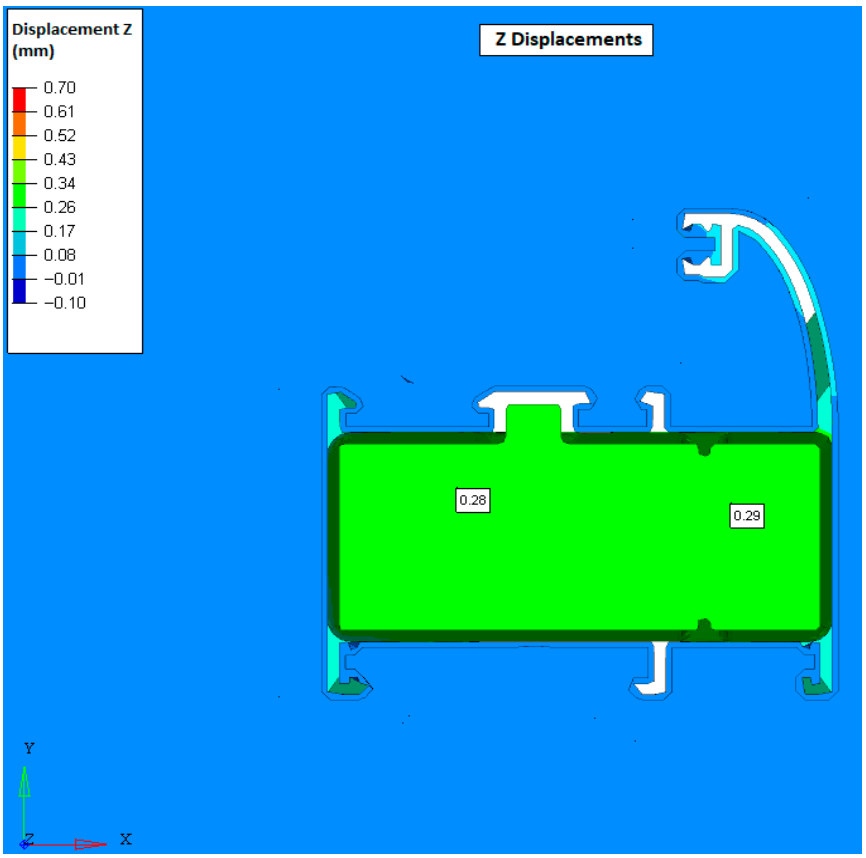


**Figure 15.** Displacement (Z) for the initial die design of Die 1.

The modifications selected to improve the extrusion process are illustrated in Figure 16 and summarized below. The boundary conditions for the FEA of the optimized aluminum extrusion die for Die 1 were established using a refined mesh and updated thermal settings. After a mesh convergence analysis, the final model consisted of 901,314 nodes and 3,840,602 elements. Tetrahedral elements were used for both the aluminum billet and the die plates, while a prismatic mesh was applied to the profile to better represent its geometry. Thermal conditions were defined by heating the billet to 470 °C, maintaining the die at 500 °C, and setting the container to 430 °C, thereby replicating realistic extrusion conditions.

The billet length was set to 1000 mm, and the ram speed was evaluated at two levels (6.7 mm/s and 12 mm/s) to examine how different extrusion rates influence die behavior and material flow. This comprehensive configuration enables accurate simulation of the extrusion process and supports a reliable assessment of die design performance under varying operational conditions. The same boundary and symmetry boundary conditions for the FEA of the optimized die design were also applied as in the previous simulation. The number of nodes and elements have also been increased to 901,314 and 3,840,602 respectively. The die modifications include reducing the die entry surface to improve material flow and to limit the tendency of the extrudate to shift toward the bottom center of the die. Adjustments to the bearing dimensions are introduced to promote more uniform flow and to increase material velocity at the top of the curved segment of the profile. Finally, changes to the bridge dimensions are proposed to reduce mandrel displacement in the Y-direction. Collectively, these modifications aim to enhance both the efficiency and the quality of the extrusion process. Each modification of the optimized die was directly guided by the FEA results of the initial design. The large exit-speed variation (52%) and the downward flow tendency identified in Figure 12 motivated the reduction in the die entry surface to redistribute material flow and counteract the inward shift of the extrudate. The bearing adjustments were introduced to correct the low velocities (Figure 11) of the curved part of the profile. Finally, the bridge geometry was modified to reduce the mandrel displacement predicted in the Y- and Z-directions (Figures 14 and 15), thereby improving alignment and stabilizing the welding-chamber flow. These targeted changes directly address the key FEA indicators and form the basis of the optimized die design.

### *3.3. Optimized Die Design Simulation Results*

Following the previously described modifications to the die design, two additional analyses were performed. Both analyses used identical extrusion conditions, with the only difference being the use of a ram speed of 12 mm/s in the second analysis. This adjustment allowed for the evaluation of the die and extrudate behavior under substantially higher extrusion speeds.

Figures 17–22 show the results for the ram speed of 6.7 mm/s. With respect to the relative exit speed difference (excluding the top of the curved portion of the extrudate), the difference between the maximum and minimum values decreased by 44.2%, as illustrated in Figure 17. The temperatures at the bearings remained stable, as shown in Figure 18. The displacement in the Y-direction decreased from 0.02 mm to 0.01 mm, representing a significant reduction, as shown in Figure 22. However, the displacement in the Z-direction, presented in Figure 23, increased slightly from 0.29 mm to 0.30 mm—an increase of 5.3%.

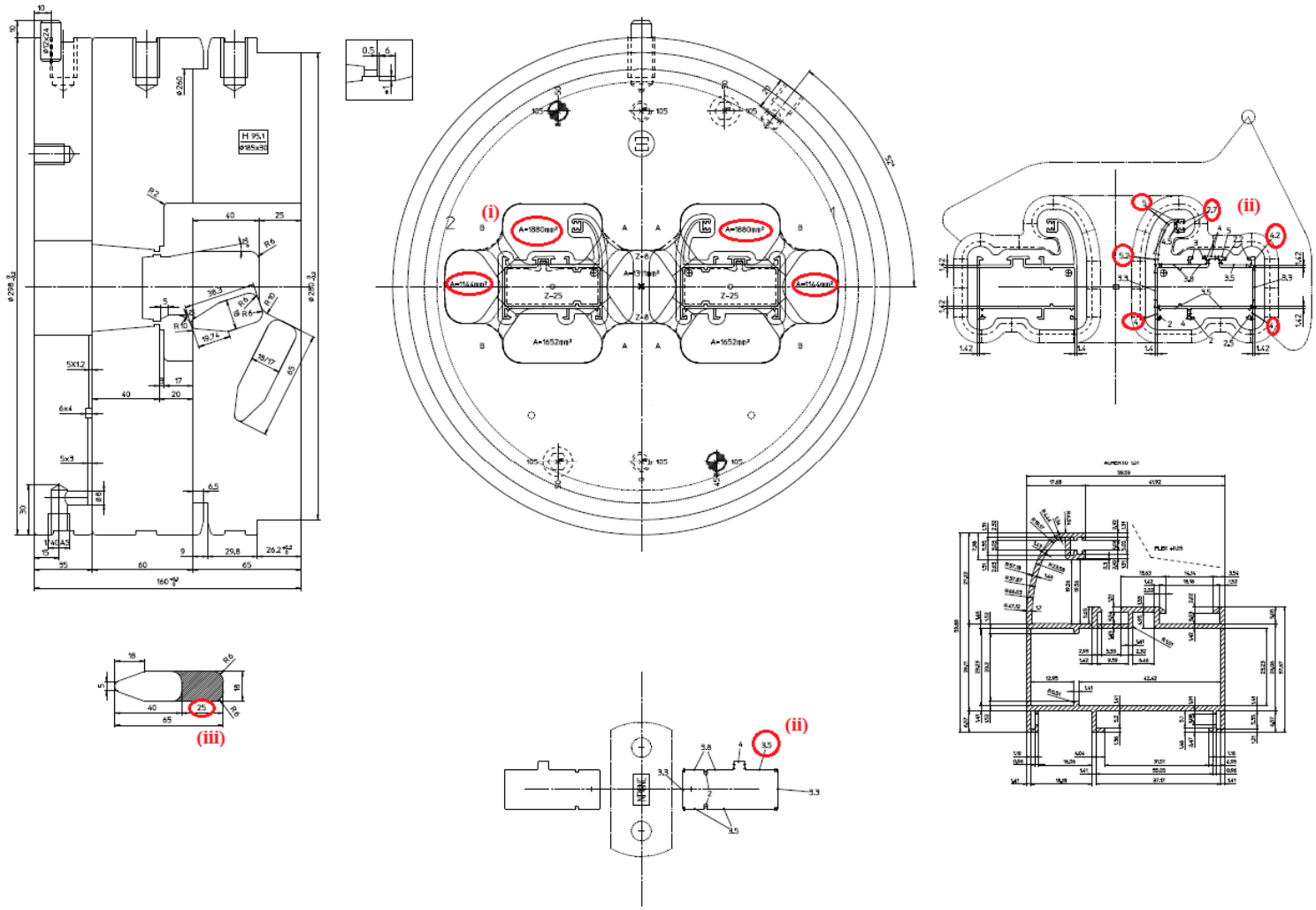


**Figure 16.** Technical drawing for the enhanced die design of extrudate with Die 1. (i) Reduction in the die entry surface, (ii) Bearing adjustment and (iii) Modification in the bridge geometry.

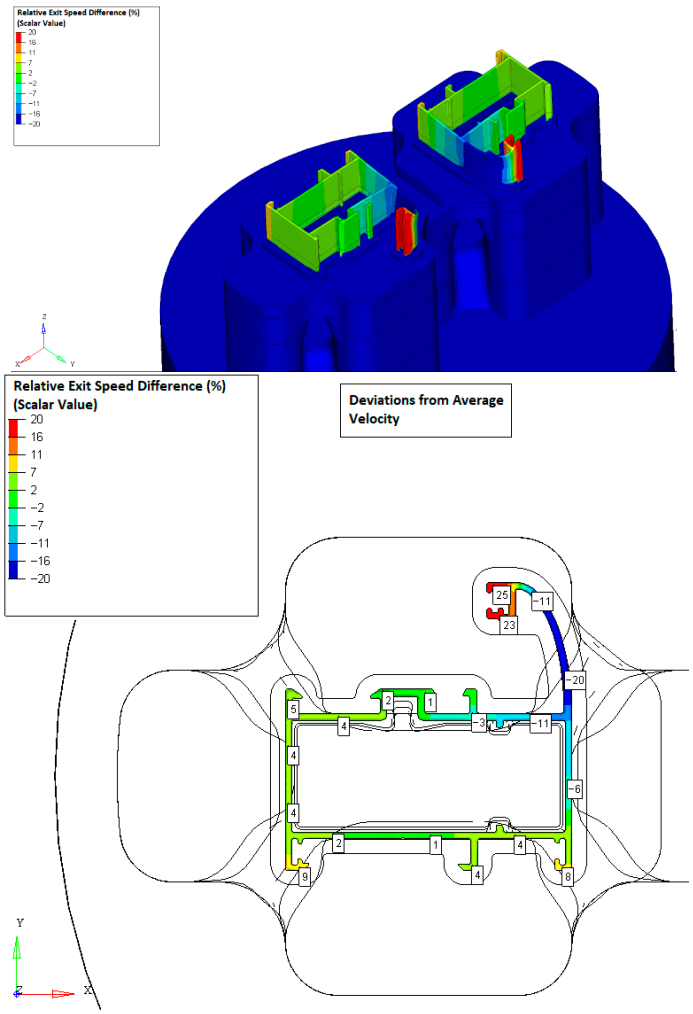


**Figure 17.** Relative exit speed difference for the optimized die design of Die 1 at ram speed of 6.7 mm/s.

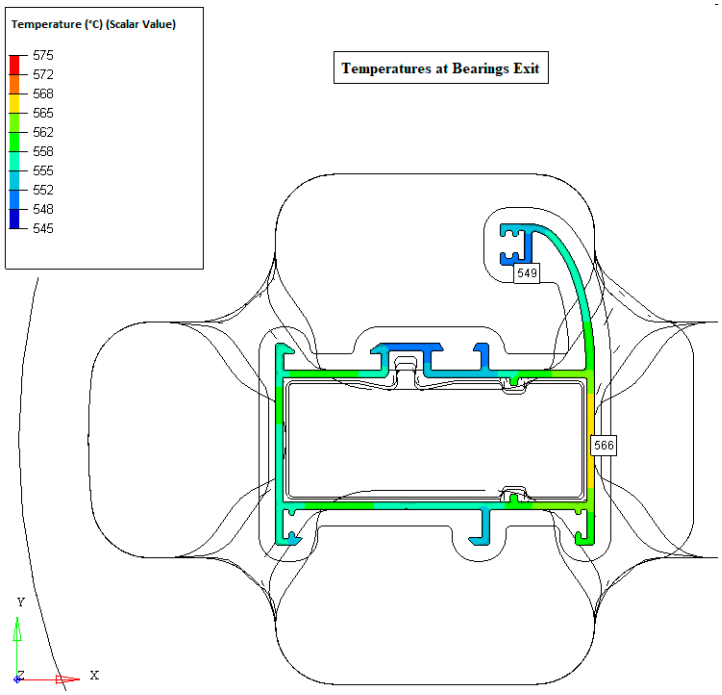


**Figure 18.** Temperatures at bearing exit for the optimized die design of Die 1 at ram speed of 6.7 mm/s.

https://doi.org/10.3390/app16052385

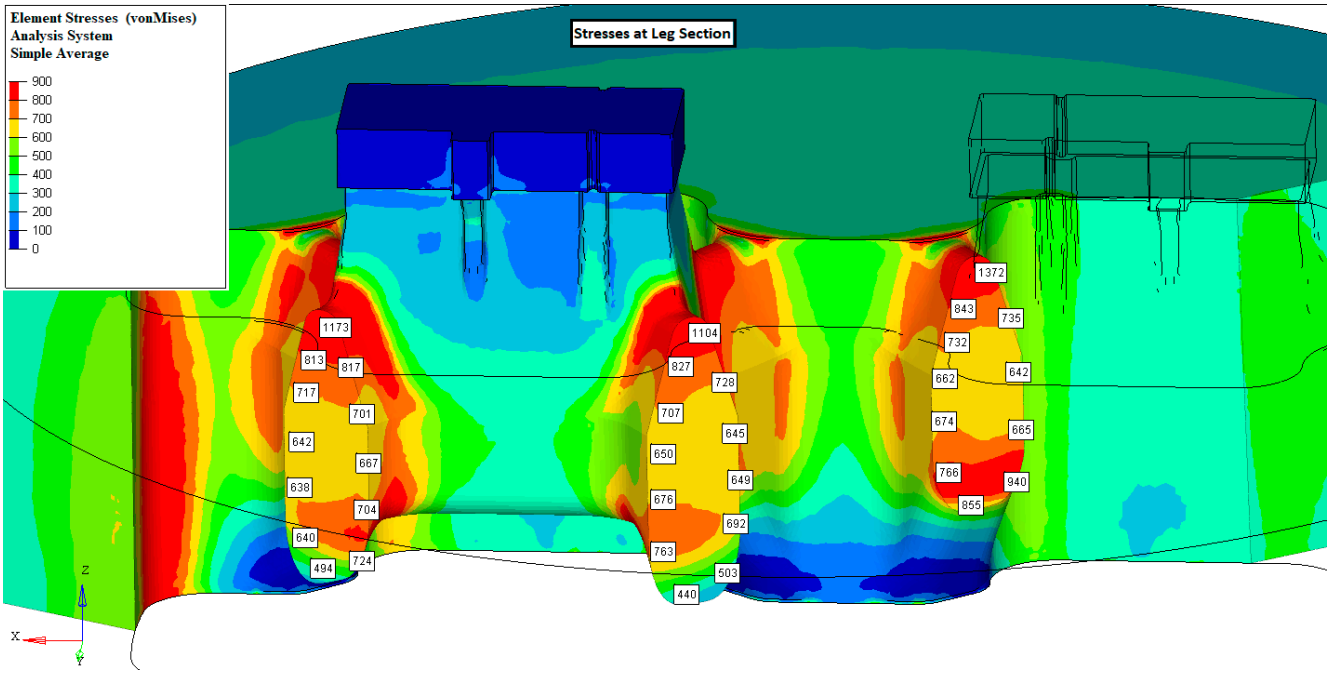


**Figure 19.** Von Mises stresses on the leg section for the optimized die design of Die 1 at ram speed of 6.7 mm/s.

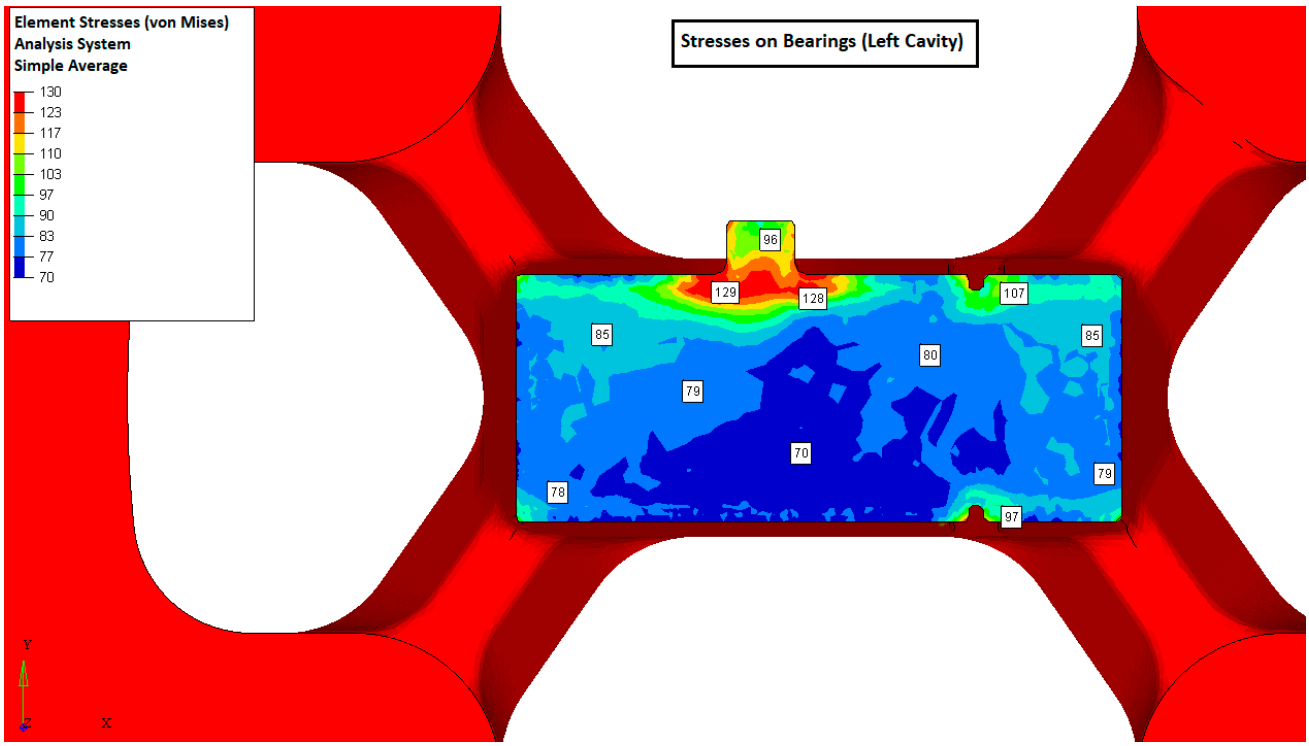


**Figure 20.** Von Mises stresses on bearings at the left cavity for the optimized die design of Die 1 at ram speed of 6.7 mm/s.

https://doi.org/10.3390/app16052385

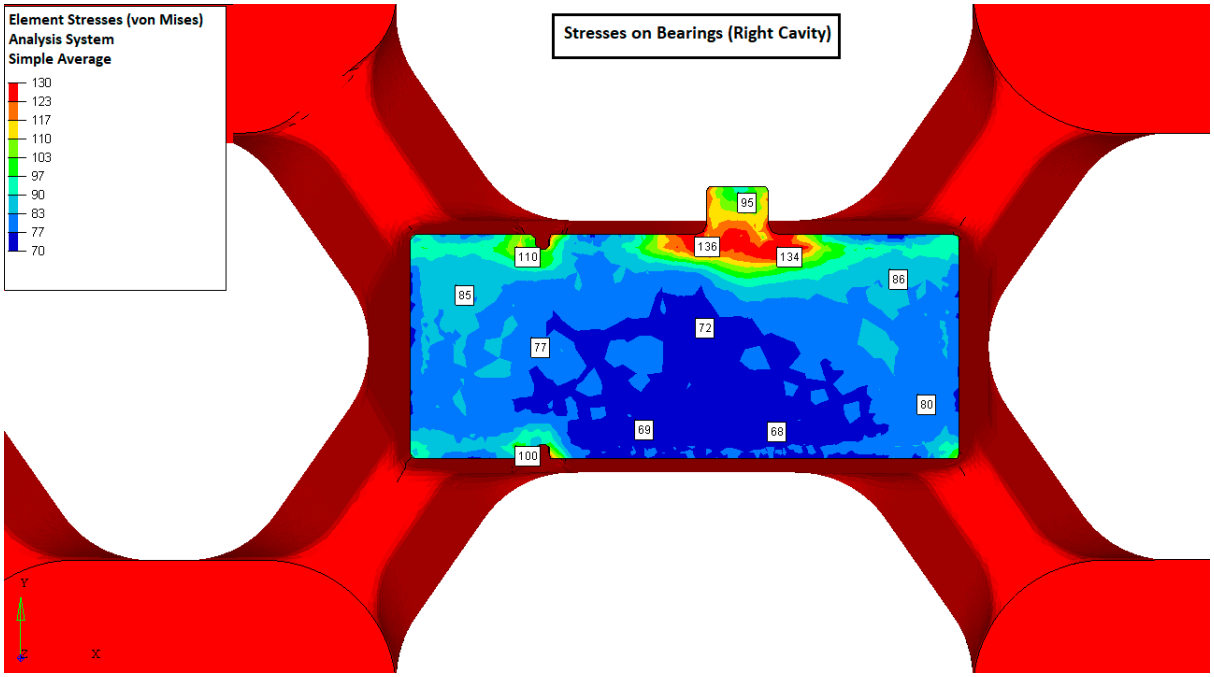


**Figure 21.** Von Mises stresses on bearings at the right cavity for the optimized die design of Die 1 at ram speed of 6.7 mm/s.

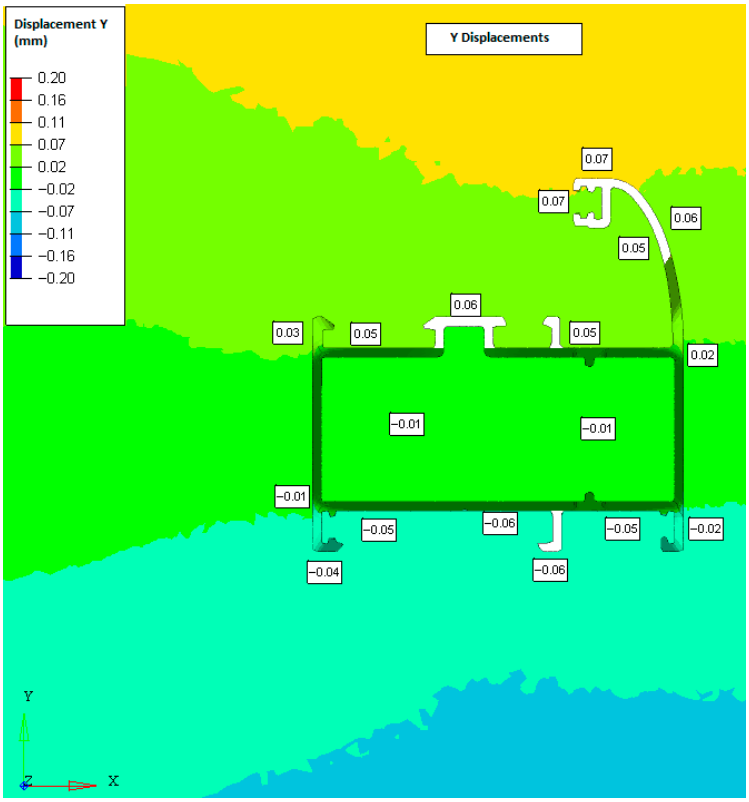


**Figure 22.** Displacement (Y) for the optimized die design of Die 1 at ram speed of 6.7 mm/s.

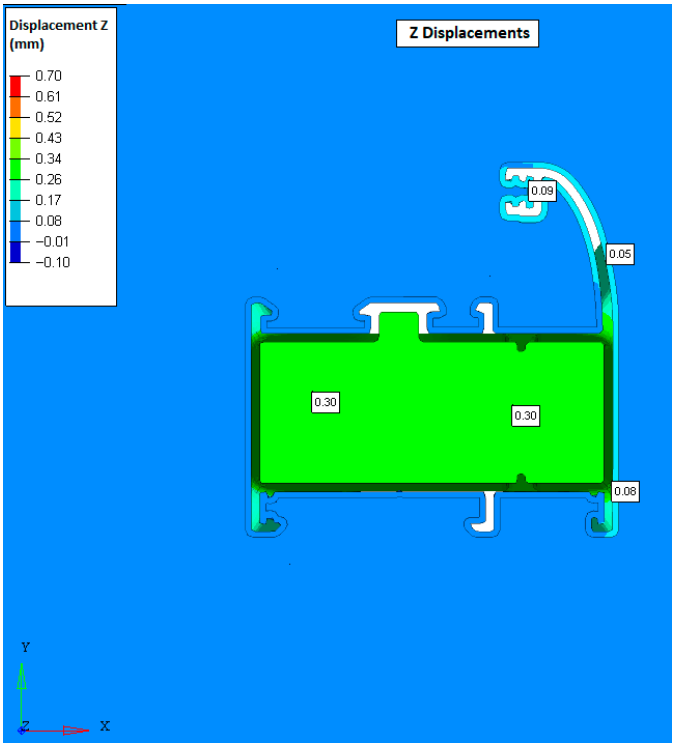


**Figure 23.** Displacement (Z) for the optimized die design of Die 1 at ram speed of 6.7 mm/s.

For the behavior of the extrusion process at increased ram speeds, Figures 24–30 show the simulation results for the initial die design (Die 1) and the optimized die design, with the only difference being the implementation of a ram speed of 12 mm/s instead of 6.7 mm/s. The relative exit speed difference increased by 17%, from 29% to 34%. The temperatures at the bearings rose by 2.55–2.65%, equivalent to an increase of 15 °C. The displacements in the Y and Z directions remained unchanged, as demonstrated in Figures 29 and 30.

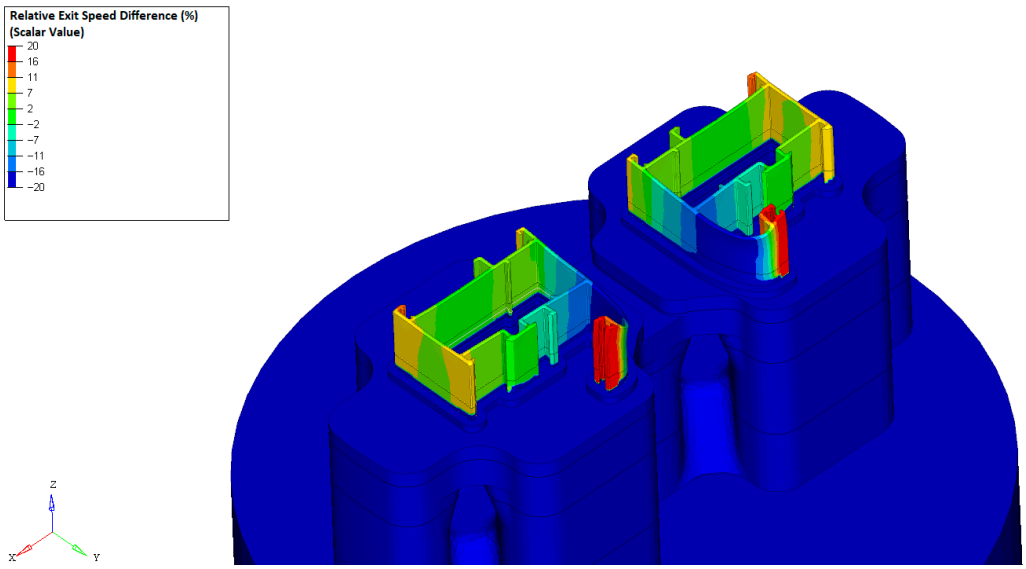

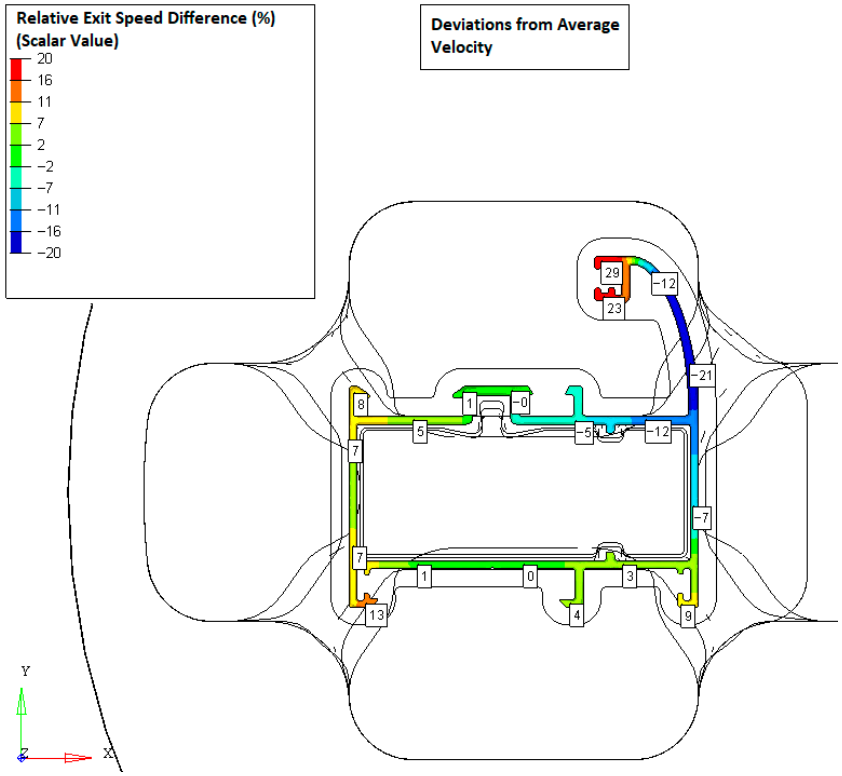


**Figure 24.** Relative exit speed difference for the optimized die design of Die 1 at ram speed of 12 mm/s.

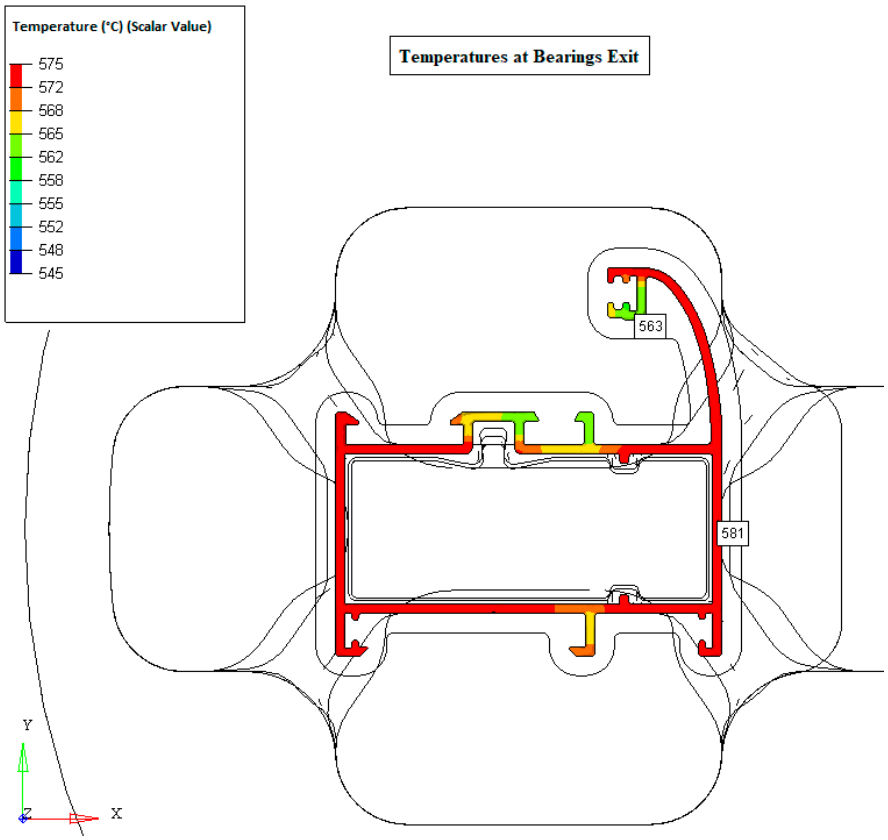


**Figure 25.** Temperatures at the bearing exit for the optimized die design of Die 1 at ram speed of 12 mm/s.

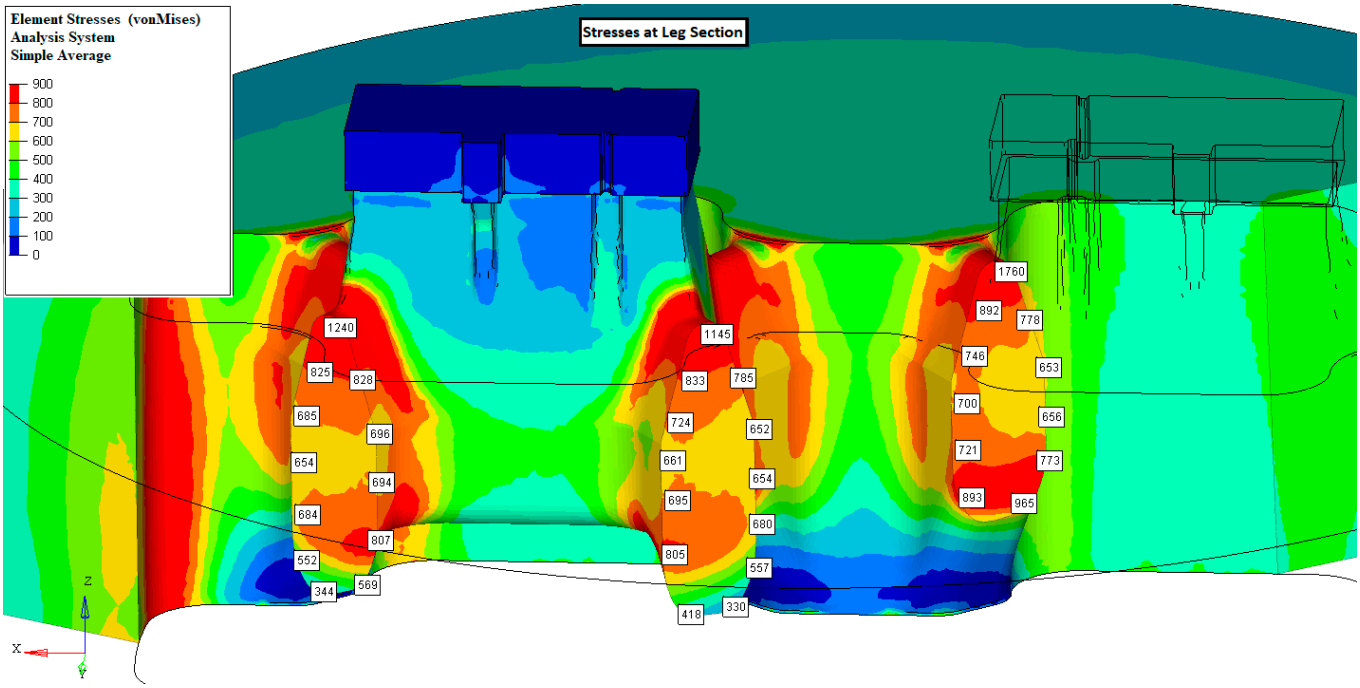


**Figure 26.** Von Mises stresses at the leg section for the optimized die design of Die 1 at ram speed of 12 mm/s.

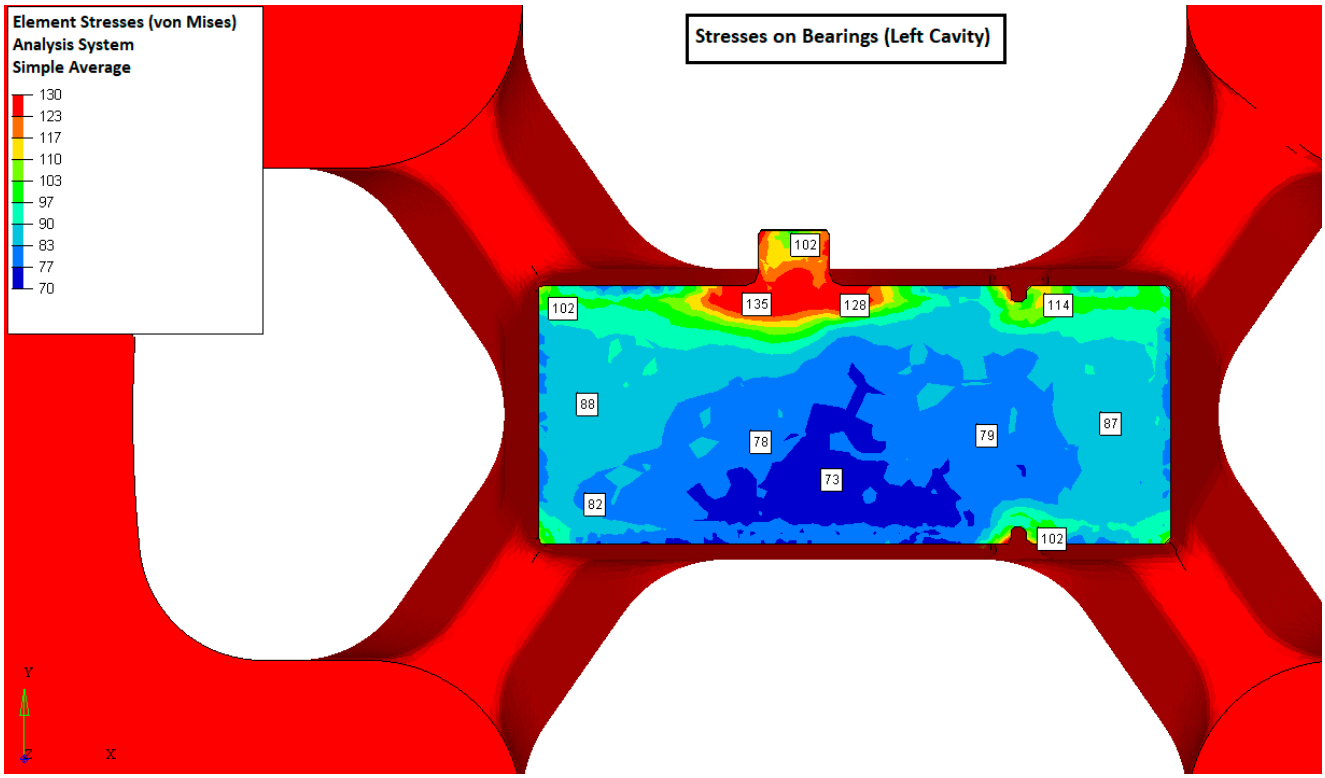


**Figure 27.** Von Mises stresses on bearings at the left cavity for the optimized die design of Die 1 at ram speed of 12 mm/s.

https://doi.org/10.3390/app16052385

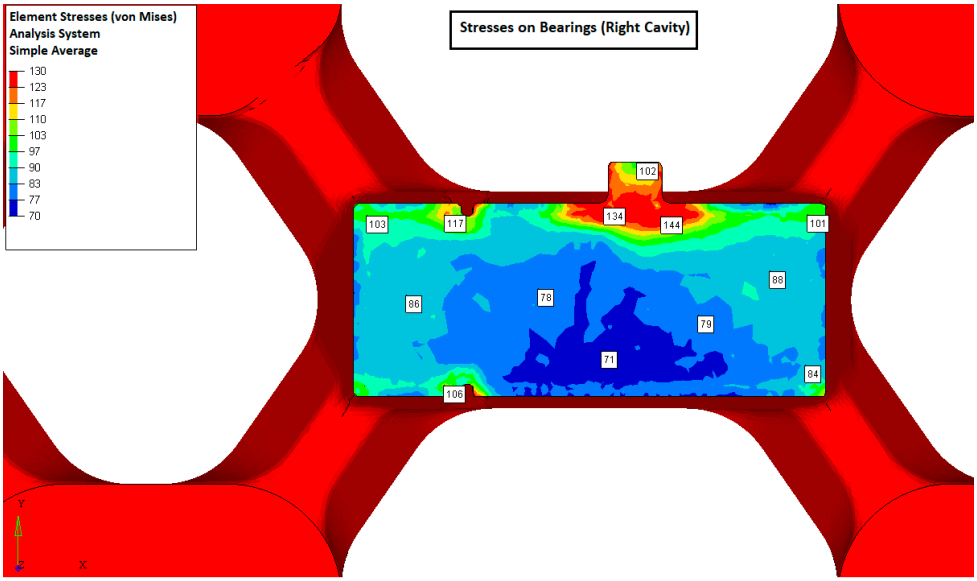


**Figure 28.** Von Mises stresses on bearings at the right cavity for the optimized die design of Die 1 at ram speed of 12 mm/s.

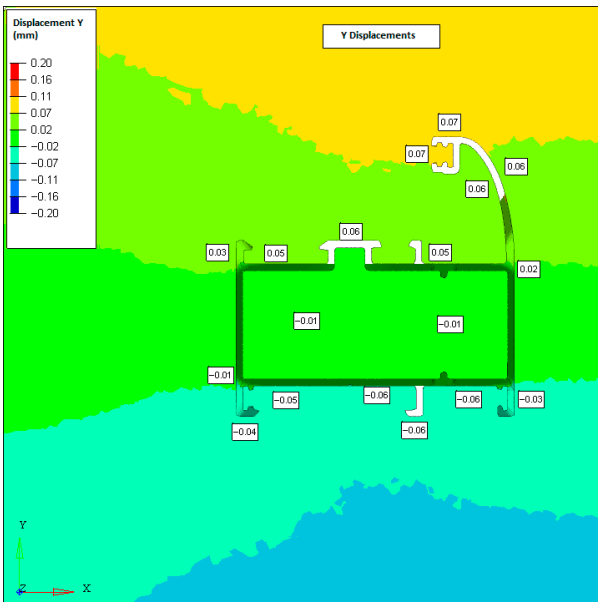


**Figure 29.** Displacement (Y) for the optimized die design of Die 1 at ram speed of 12 mm/s.

In addition to these comparisons, it is important to create comparative chart diagrams for the results presented in Figures 19–21 and Figures 26–28. These figures provide information about the von Mises stresses on the leg sections and the bearing. In the HyperXtrude simulations, the von Mises yield criterion is used to evaluate the material's response under the complex multiaxial stress state that develops during aluminum extrusion. The von Mises-equivalent stress provides a single scalar measure of the distortion energy, allowing us to identify regions where the local stress state approaches or exceeds the alloy's yield strength. This helps assess the onset of plastic deformation within the billet and die-bearing regions, which is essential for interpreting flow behavior, predicting potential defects, and understanding the overall deformation mechanics during extrusion. Consequently, they offer significant insights into the effect of ram speed on the resulting stresses. Figure 31 illustrates the evolution of von Mises stresses on the leg sections for both simulated ram speeds. The leg geometry was divided into outside and middle sections, with the middle portion further split into large and small

regions. A comparison of the maximum stress values presented in Figures 19 and 26 shows that the overall stress distribution pattern among the three legs remained consistent. However, the small middle leg section exhibited a notably higher increase in maximum von Mises stress—16.96% and 24.28% at a ram speed of 6.7 mm/s, and 41.94% and 53.72% at a ram speed of 12 mm/s—compared with the outside leg and the larger middle section, respectively. Furthermore, the 79% increase in ram speed (from 6.7 mm/s to 12 mm/s) resulted in increases of 5.71%, 3.71%, and 28.28% in von Mises stress for the outside leg, large middle leg, and small middle leg sections, respectively.

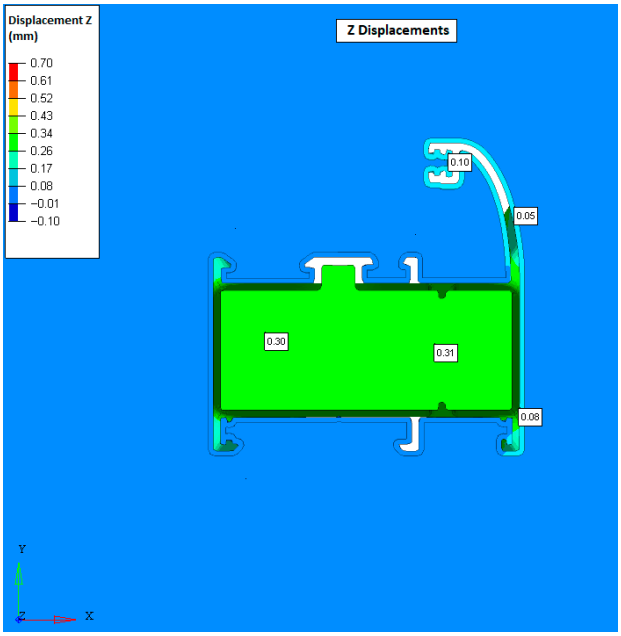


**Figure 30.** Displacement (Z) for the optimized die design of Die 1 at ram speed of 12 mm/s.

The von Mises stress values obtained from the FEA appear not to exceed the yield strength of H13 and H11 hot-work tool steels, which are commonly used for aluminum extrusion dies. At 500 °C, the yield strengths of these steels range from approximately 1000 to 1155 MPa, with only two localized points on the leg sections surpassing these limits. Although these overstressed regions are limited in extent, they indicate that operating at the highest tested ram speed (12 mm/s) brings the die very close to its material limits. Such localized exceedances can act as initiation sites for thermal-fatigue cracking and accelerated wear during repeated extrusion cycles. For this reason, a lower ram speed of 9.5 mm/s was selected as a conservative upper operating limit. This value maintains a sufficient safety margin relative to the observed stress trend, ensuring long-term die integrity while still providing a meaningful increase in productivity. Von Mises stress distributions on the bearings for the left and right cavities at both simulated ram speeds are shown in Figure 32. Similar to the leg sections, the stress behavior of the two cavities is consistent. Comparing the maximum stress values in Figures 19, 20, 26 and 27 shows that the maximum von Mises stresses at point 3 increased by 4.65% in the left cavity and 7.46% in the right cavity when the ram speed was raised by 79% (from 6.7 mm/s to 12 mm/s). Meanwhile, the maximum stresses at point 5 remained nearly unchanged. Overall, the maximum von Mises stresses for both cavities increased by an average of 5.37% across the two speeds. These two values correspond to the two principal peaks in Figure 32a,b. Finally, Figure 32c illustrates the method used to map the sequence of stresses for Die 1 in Figures 31 and 32, based on the data derived from Figures 19–21 and 26–28.

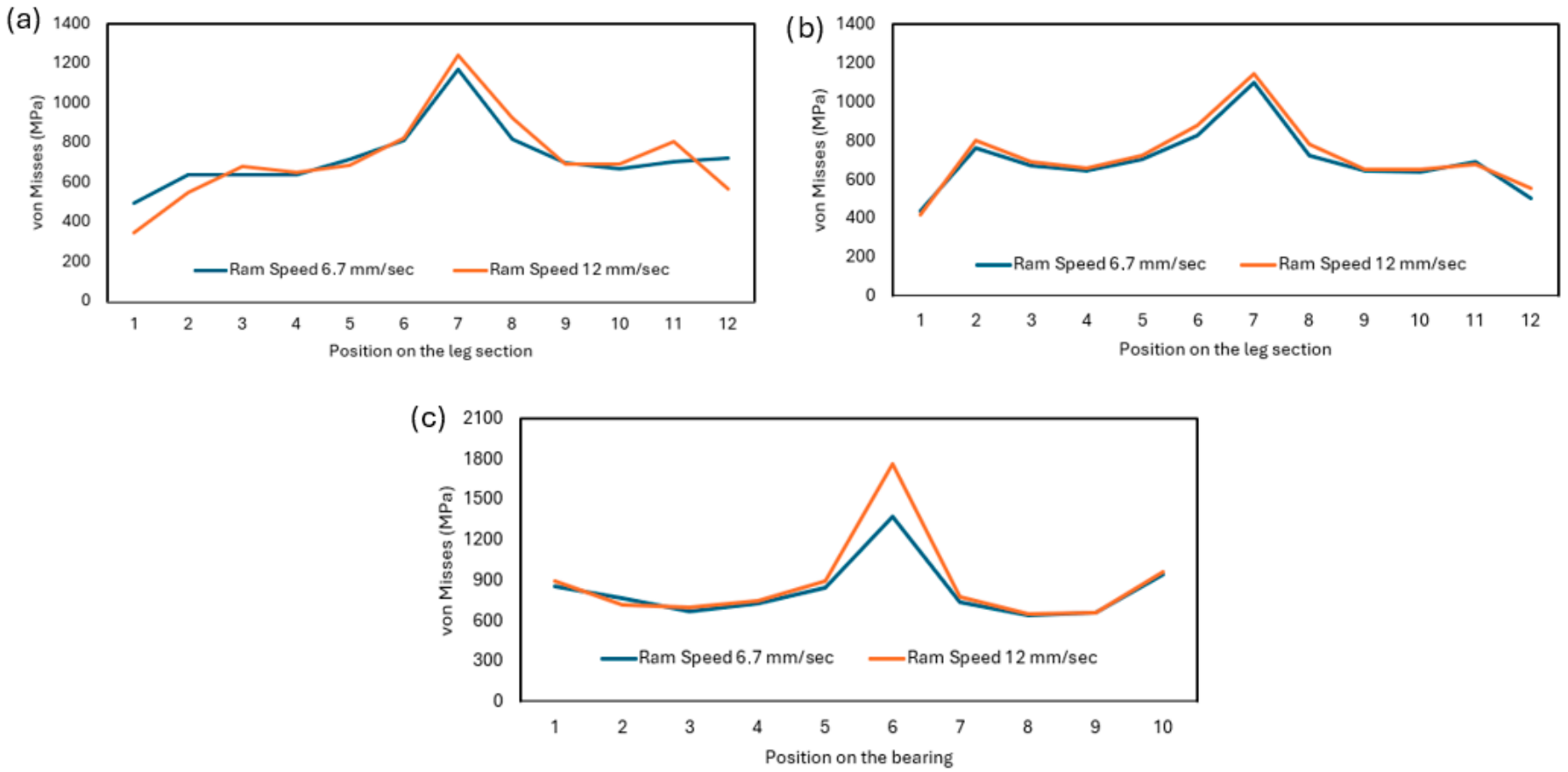


**Figure 31.** Comparison of von Mises stresses for both simulated speeds on the (**a**) outside leg section, (**b**) middle leg section (large) and (**c**) middle leg section (small).

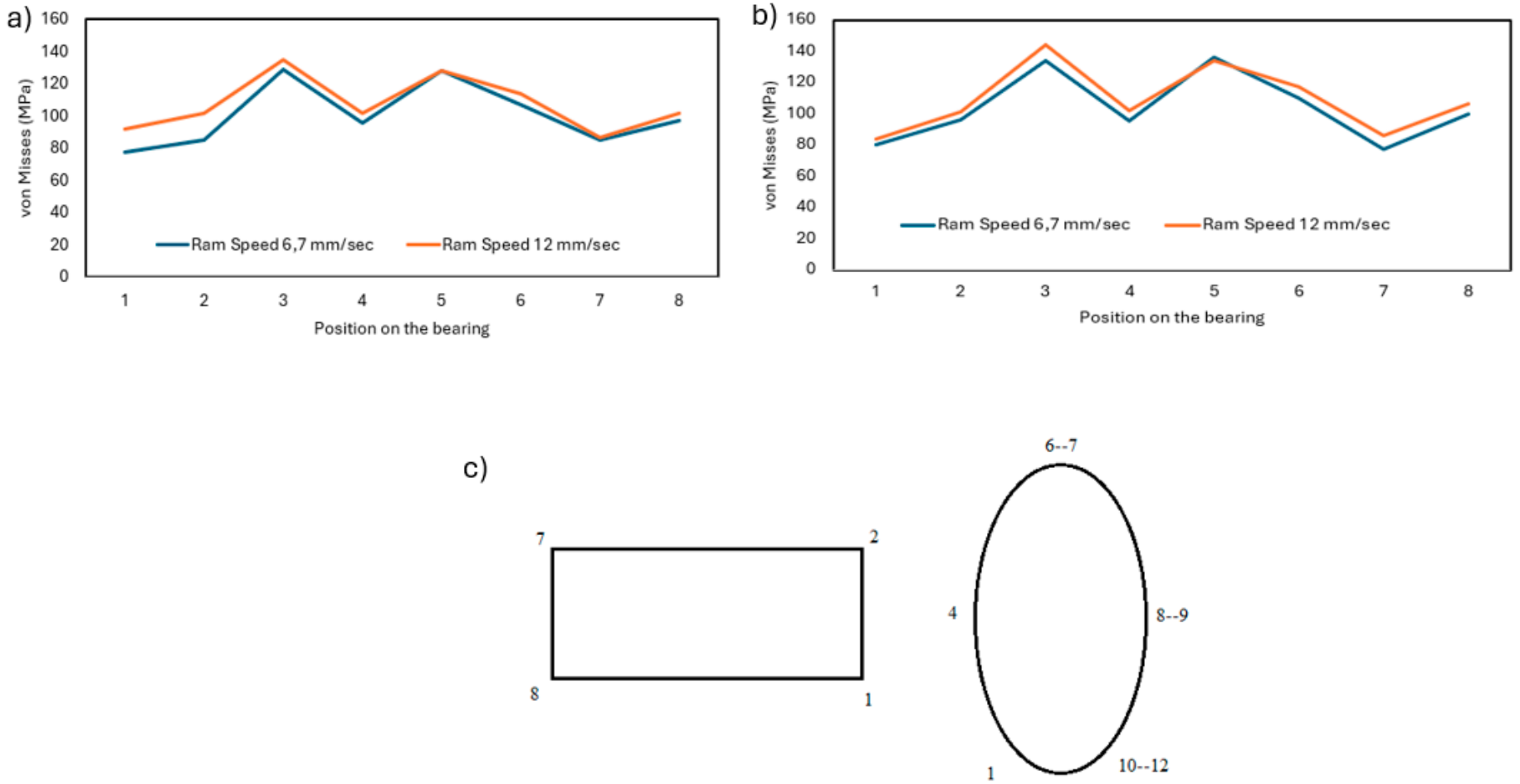


**Figure 32.** Comparison of von Mises stresses for both simulated speeds on the (**a**) bearings for left cavity, (**b**) bearings for right cavity and (**c**) von Mises stress sequence visualization for Die 1. Numbers 1-12 represent the method used to map the sequence of stresses.

## 4. Validation Process for the FEA Models

The subsequent phase of the methodology involved validating the FEA models. The workflow follows an industrial single-pass optimization approach, where the initial die performance is evaluated, the optimized design is developed through FEA, and the final validation is carried out on the manufactured optimized die. This process entailed fabricating the die and extruding aluminum billets to corroborate specific FEA predictions. Ultimately, the extrusion results were analyzed to assess the enhancement in productivity efficiency achieved by employing liquid nitrogen as a cooling agent in the new die design. The die was manufactured in accordance with the technical drawings shown in Figure 16. Producing an aluminum extrusion die is a highly specialized procedure that integrates advanced material selection, precision machining, and thermal treatment to ensure reliable performance under the demanding conditions of extrusion. Such dies are typically made from high-performance tool steels—most commonly H13—due to their superior resistance to thermal fatigue, wear, and mechanical loading. The fabrication process begins with selecting the appropriate steel block and performing rough machining. This is followed by high-precision CNC milling and electrical discharge machining (EDM) to form the die's intricate features, such as bearing surfaces, flow channels, and welding chambers in the case of porthole dies. After the geometry is fully defined, the die undergoes controlled heat treatment to increase hardness and improve mechanical strength. The initial extruded sections and their corresponding FEA results are shown below. Figure 33 illustrates the mandrel of the die.

**Figure 33.** Mandrel of Die 1.

The FEA models were validated after the initial extrusions using the previously described die, with extrusion parameters selected in accordance with Figure 10. The resulting extruded sections and their corresponding FEA outputs are presented below, demonstrating a strong agreement between simulation and experiment. Figure 34 confirms the validity of the simulation results discussed in this research paper, showing

that they can be effectively applied to optimize similar die design methodologies. The left portion of Figure 34 displays the relative exit speed variation (%) of the extrudate, while the right portion shows the actual extrudate exiting the press. The areas highlighted in blue—predicted to have lower exit speeds—and those in red—predicted to exit faster—correspond closely with the behavior observed during the production trials.

Furthermore, Figure 35 presents the extrudates measured after stretching, along with a comparison between their final dimensions and the specified target dimensions. This evaluation was carried out using the EngView Packaging Suite 2022 (EngView Systems, Sofia, Bulgaria), a comprehensive software and hardware system designed to ensure highly accurate dimensional verification. The suite includes the Scan Fit and Measure (SFM) module, an advanced 2D quality control solution widely used for assessing extruded aluminum and PVC profiles. Utilizing flatbed scanner technology, SFM performs precise, non-contact measurements of critical parameters such as size, position, wall thickness, and Geometric Dimensioning and Tolerancing (GD&T). By comparing scanned profiles directly with CAD models, the system provides immediate PASS/FAIL results and detailed visual deviation maps. Its high measurement accuracy, rapid scanning capability, and integrated data management tools make it particularly valuable for ensuring dimensional compliance, reducing production variation, and improving traceability in extrusion quality control.

The measurement results clearly show that the final extrudate dimensions fully meet the required tolerances, with the maximum deviation from the nominal geometry being 0.19 mm. This quantitative agreement between the measured profile and the FEA-predicted shape demonstrates that the numerical model provides sufficiently accurate predictions of the material flow and final dimensions, supporting its validity for the analyses presented in this work. All measurements were carried out in accordance with EN 755-9, Aluminium and aluminium alloys—Extruded rod/bar, tube and profiles—Part 9: Profiles, tolerances on dimensions and form [32].

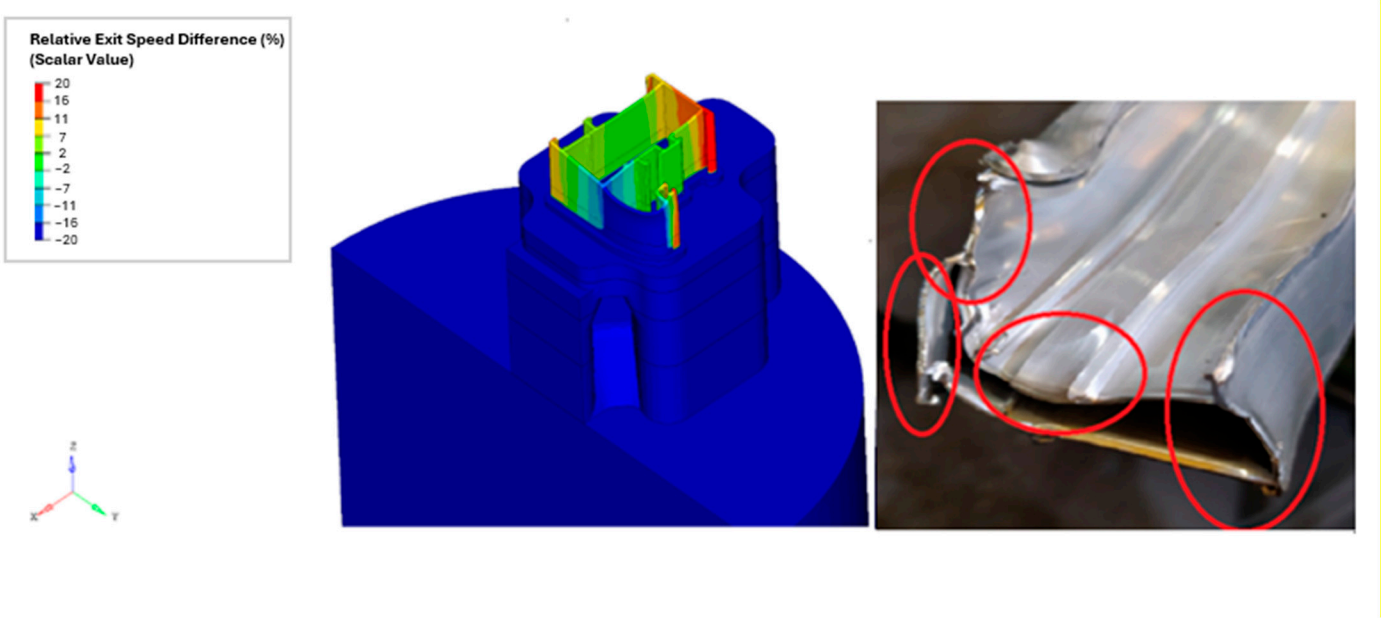


**Figure 34.** Comparison between the FEA results and the extruded sections from the beginning (Die 1). The red circles indicate the parts of the extrudate that are in absolute correlation with the FEA results.

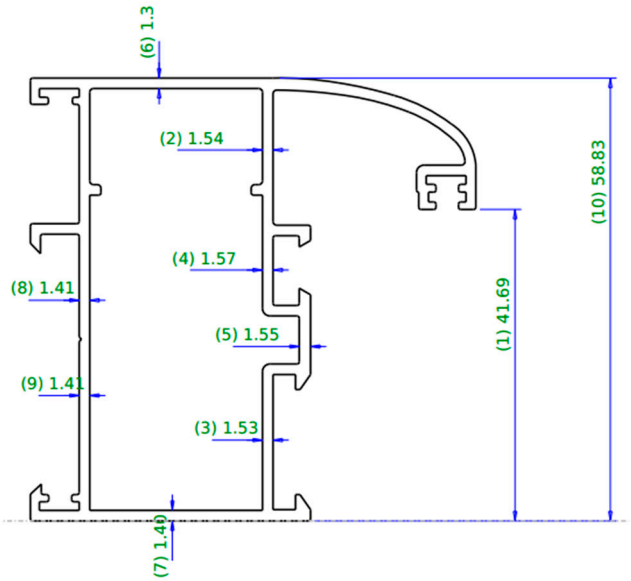


| Step ID | Label | Nominal | Tolerance | Actual | Deviation | Evaluation |
|---|---|---|---|---|---|---|
| 1 | | 41.50 | +/−0.5000 | 41.69 | 0.19 | OK |
| 2 | | 1.40 | +/−0.2500 | 1.54 | 0.14 | OK |
| 3 | | 1.40 | +/−0.2500 | 1.53 | 0.13 | OK |
| 4 | | 1.40 | +/−0.2500 | 1.57 | 0.17 | OK |
| 5 | | 1.50 | +/−0.2500 | 1.55 | 0.05 | OK |
| 6 | | 1.40 | +/−0.2500 | 1.35 | 0.05 | OK |
| 7 | | 1.40 | +/−0.2500 | 1.40 | 0.00 | OK |
| 8 | | 1.40 | +/−0.2500 | 1.41 | 0.01 | OK |
| 9 | | 1.40 | +/−0.2500 | 1.41 | 0.01 | OK |
| 10 | | 59.00 | +/−0.5000 | 58.83 | 0.17 | OK |

**Figure 35.** SFM dimensions measurement for Die 1.

## 5. Production Data with Liquid Nitrogen Use for Optimized Die Design

After fabricating the optimized die design, the extrusion process was carried out, with the results shown in Figures 36 and 37. The process parameters and the chemical composition of the alloy were kept the same as those used in the initial die designs. The updated extrusion parameters are summarized in Table 2. It was observed that the efficiency for Die 1 increased by 8.76% (from 84.5% to 91.9%), a notable improvement attributed to the combination of the new die design and the application of liquid nitrogen. Liquid nitrogen was supplied from an external storage tank located approximately 70 m from the extrusion line. The nitrogen was delivered through a 15 mm diameter pipeline at a pressure of 7 bar. Before entering the die, the nitrogen passed through a sub-cooling unit to ensure it remained in a liquid state, reaching temperatures below −200 °C at the die inlet. The maximum flow capacity of the system, as specified by the manufacturer, is 75 kg/h when the control valve is fully open. The temperatures of the first three zones of the billet preheating oven are also listed in the table above. These first three zones are illustrated clearly in Figure 7 of Section 2.3. The use of liquid nitrogen began at billet number 4, with the corresponding ram speeds indicated by red values. The effect of the die redesign and the effect of liquid-nitrogen cooling can be clearly distinguished. The new die geometry alone resulted in a 14.7% increase in ram speed, raising the stable operating speed from 6.8 mm/s to 7.8 mm/s. When liquid nitrogen cooling was subsequently introduced, an additional 21.8% increase was achieved, allowing the ram speed to reach 9.5 mm/s. This separation shows that the structural optimization of the die primarily improved flow balance and reduced bearing-related resistance, whereas the $LN_2$ cooling mainly enhanced thermal stability and reduced exit temperatures, enabling

higher speeds without exceeding thermal or mechanical limits. Ram pressure, however, was only minimally affected by either modification, indicating that the improvements were driven by geometric and thermal effects rather than changes in overall process load. Figure 38 shows the evolution of ram speed and the exit temperature of the extrudates for both the initial and optimized die designs. The billet where liquid nitrogen was applied is marked with red numbers. The main observation from these figures is that the significant rise in ram speed did not affect the exit temperature of the extrudates, due to the cooling effect of the liquid nitrogen. Specifically, increasing ram speed from 6.7 mm/s to 9.5 mm/s seems to have no noticeable effect on the exit temperature, whereas the application of liquid nitrogen produces a slight decrease in exit temperature, as indicated by the light orange trend line. To clarify the link between cooling and speed capability, it is important to note that the maximum allowable ram speed is limited by the exit-temperature threshold of the alloy, above which surface defects and die-soldering become likely. The application of liquid nitrogen reduced the exit temperature by approximately 8 °C, creating an additional thermal margin that allowed the ram speed to increase from 7.8 mm/s to 9.5 mm/s, without exceeding the critical temperature limit. In other words, the temperature reduction directly expanded the safe operating window, enabling higher deformation rates while maintaining thermal stability at the die exit.

**Table 2.** Production data for initial die design for extrudate with Die 1.

| Profile Code | Billet Length (mm) | Temp. at Zone 1 (°C) | Temp. at Zone 2 (°C) | Temp. at Zone 3 (°C) | Efficiency |
|---|---|---|---|---|---|
| 1 | 1000 | 470 | 450 | 430 | 91.90% |

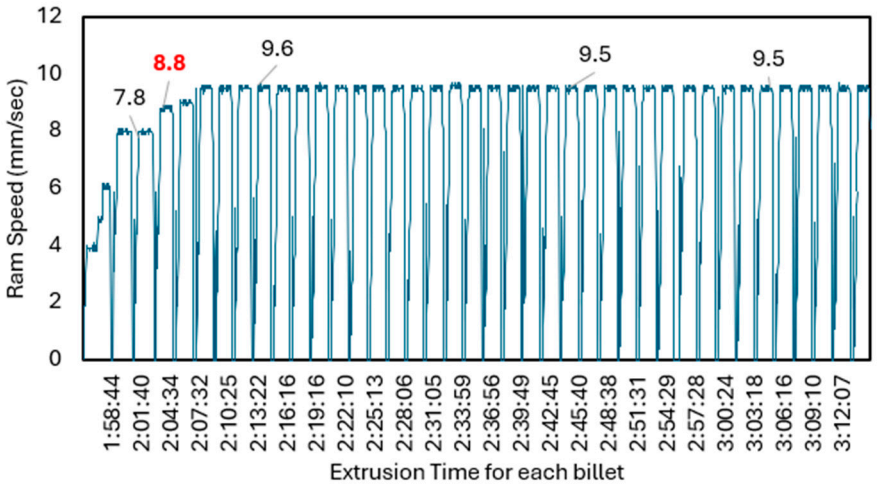


**Figure 36.** Ram speed for optimized die design for extrudate with Die 1. Red color indicates the billet where liquid nitrogen was applied.

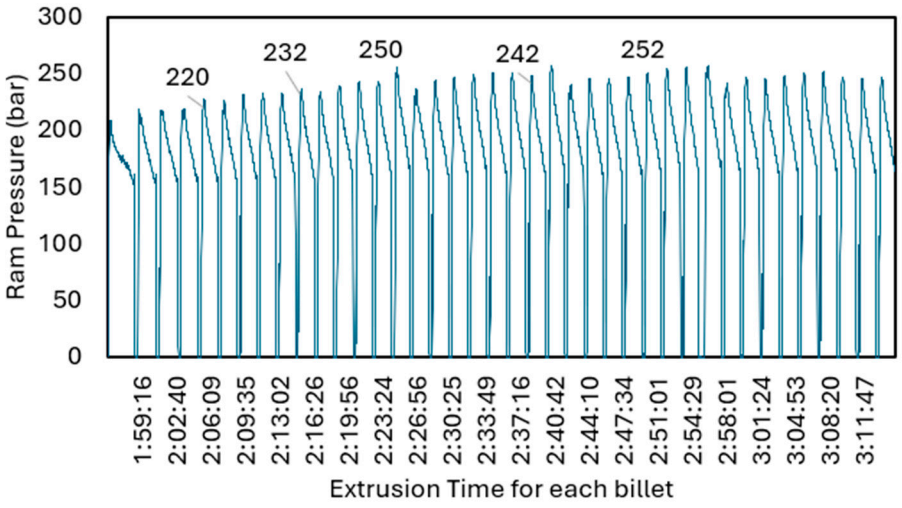


**Figure 37.** Ram pressure for optimized die design for extrudate with Die 1.

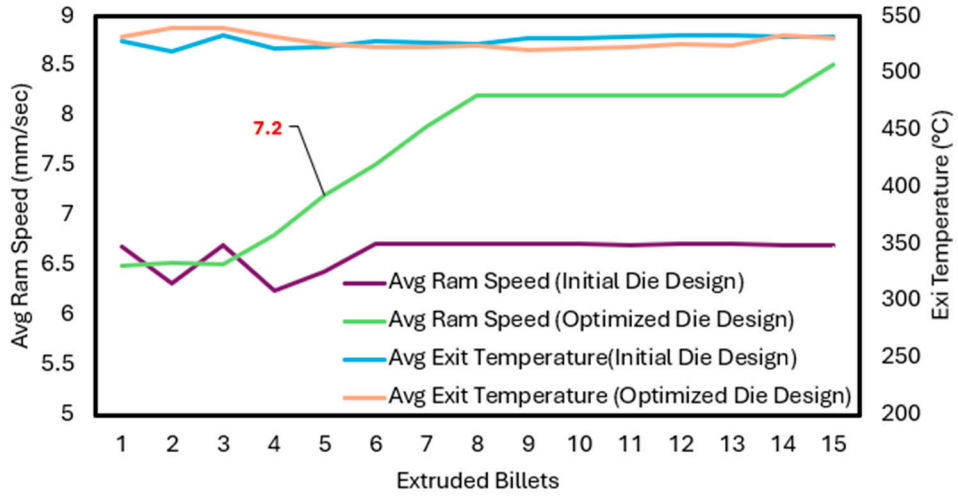


**Figure 38.** Average ram speed and exit temperature for Die 1. Red color indicates the billet where liquid nitrogen was applied.

## 6. Conclusions

In this study, a porthole die with two holes and an extrusion ratio of 70.16 was investigated. The AA6060 alloy was chosen for both numerical and experimental analyses, with HyperXtrude™ 2022 software employed during the FEA stage. The main goal was to achieve higher productivity through improved die design structures. The combined use of FEA and liquid nitrogen was found to significantly enhance overall extrusion efficiency. The results show that the FEA predictions closely match the production outcomes regarding the shape of the extrudates at the die exit, thereby validating both the models and the methodology. Production results revealed an 8.76% increase in efficiency (from 84.5% to 91.9%), attributed to the new die design and the application of liquid nitrogen. The die design alone increased ram speed by 14.7% (from 6.8 mm/s to 7.8 mm/s), while the use of liquid nitrogen further increased ram speed by 21.8% (from 7.8 mm/s to 9.5 mm/s). Ram pressure was only minimally influenced by these modifications, and the increase in ram speed did not affect the exit temperature of the extrudates, due to the cooling provided by the liquid nitrogen system. The introduction of the new approach for measuring extrusion efficiency should also be emphasized, as it offers a more accurate way for other extruders to evaluate their process efficiency.

**Author Contributions:** Conceptualization, E.G. and D.T.; methodology, E.G.; software, E.G., P.T. and T.P.; validation, E.G., I.T. and D.T.; formal analysis, E.G., P.T. and T.P.; investigation, E.G., I.T., P.T. and T.P.; resources, P.T., T.P. and D.T.; data curation, E.G., I.T., P.T. and T.P.; writing—original draft preparation, E.G., I.T. and P.T.; writing—review and editing, T.P. and D.T.; visualization, E.G. and T.P.; supervision, D.T.; project administration, P.T. and D.T.; funding acquisition, E.G. All authors have read and agreed to the published version of the manuscript.

**Funding:** This research received no external funding.

**Data Availability Statement:** Data are contained within the article.

**Conflicts of Interest:** Authors E. Giarmas and I. Theodoridis were employed by the company Alumil SA. Authors P. Tounis and T. Pinter were employed by the company Matrex Aluminum Dies S.A. The remaining authors declare that the research was conducted in the absence of any commercial or financial relationships that could be construed as a potential

## References

1. Walters, J.; Foster, M.; Bandar, A. The 'State of the Art' in Aluminum Extrusion Simulation Using the Finite Element Method. *Extrus. Technol.* **2012**, *1*, 531–541.
2. Bastani, A.F.; Aukrust, T.; Skauvik, I. Study of Flow Balance and Temperature Evolution over Multiple Aluminum Extrusion Press Cycles with HyperXtrude™ 9.0. *Key Eng. Mater.* **2010**, *424*, 257–264.
3. Engelhardt, M.; Kurmajev, S.; Maier, J.; Becker, C.; Hora, P. The Application of FEA for Optimization of Die Design. *Mater. Today Proc.* **2019**, *10*, 226–233.
4. Dong, Y.; Zhang, C.; Luo, W.; Yang, S.; Zhao, G. Material flow analysis and extrusion die modifications for an irregular and multitooth aluminum alloy radiator. *Int. J. Adv. Manuf. Technol.* **2016**, *85*, 1927–1935. https://doi.org/10.1007/s00170-016-8666-5.
5. Kloppenborg, T.; Schwane, M.; Ben Khalifa, N.; Tekkaya, A.E.; Brosius, A. Experimental and Numerical Analysis of Material Flow in Porthole Die Extrusion. *Key Eng. Mater.* **2012**, *491*, 97–104.
6. Yi, J.; Wang, Z.; Liu, Z.; Zhang, J.; He, X. FE Analysis of Extrusion Defect and Optimization of Metal Flow in Porthole Die for Complex Hollow Aluminum Profile. *Trans. Nonferrous Met. Soc. China* **2018**, *28*, 2094–2101.
7. Chen, H.; Zhao, G.Q.; Zhang, C.S.; Guan, Y.J.; Liu, H.; Kou, F.J. Numerical Simulation of Extrusion Process and Die Structure Optimization for a Complex Aluminum Multicavity Wallboard of High-Speed Train. *Mater. Manuf. Process.* **2011**, *26*, 1530–1538.
8. Zhang, C.; Zhao, G.; Guan, Y.; Gao, A.; Wang, L.; Li, P. Virtual Tryout and Optimization of the Extrusion Die for an Aluminum Profile with Complex Cross-Sections. *Int. J. Adv. Manuf. Technol.* **2015**, *78*, 927–937.
9. Truong, T.-T.; Hsu, Q.-C.; Tong, V.-C.; Sheu, J.-J. A Design Approach of Porthole Die for Flow Balance in Extrusion of Complex Solid Aluminum Heatsink Profile with Large Variable Wall Thickness. *Metals* **2020**, *10*, 553.
10. Peng, Z.; Sheppard, T. Effect of Die Pockets on Multi-Hole Die Extrusion. *Mater. Sci. Eng. A* **2005**, *407*, 89–97.
11. Sun, X.; Zhao, G.; Zhang, C.; Guan, Y.; Gao, A. Optimal Design of Second-Step Welding Chamber for a Condenser Tube Extrusion Die Based on the Response Surface Method and the Genetic Algorithm. *Mater. Manuf. Process.* **2013**, *28*, 823–834.
12. Pinter, T.; Reggiani, B.; Pelaccia, R.; Donati, L.; Negozio, M.; Didonato, S. A Novel Analytical Equation for Front Scrap Allocation in Direct Aluminum Extrusion. In Proceedings of the 12th International Aluminum Extrusion Technology Seminar (ET24), Orlando, FL, USA, 30 April–2 May 2024.
13. Saha, P. Quality Issues of Hollow Extrusions for Aerospace Applications. In Proceedings of the Ninth International Aluminum Extrusion Technology Seminar (ET 2008), Orlando, FL, USA, 13–16 May 2008; Volume 1, pp. 441–458.
14. Jowett, C.; Adams, J.; Daughetee, C.; Lea, G.; Huff, O.A.; Fossl, N. Scrap Allocation. In Proceedings of the Ninth International Aluminum Extrusion Technology Seminar (ET 2008), Orlando, FL, USA, 13–16 May 2008; Volume 1, pp. 223–244.
15. Zhang, C.; Chen, H.; Zhao, G.; Zhang, L.; Lou, S. Optimization of Porthole Extrusion Dies with the Developed Algorithm Based on Finite Volume Method. *Int. J. Adv. Manuf. Technol.* **2016**, *85*, 1901–1913.
16. Wu, X.H.; Zhao, G.Q.; Luan, Y.G.; Ma, X.W. Numerical Simulation and Die Structure Optimization of an Aluminum Rectangular Hollow Pipe Extrusion Process. *Mater. Sci. Eng. A* **2006**, *435*, 266–274.
17. Gonçalves, N.D.; Carneiro, O.S.; Nóbrega, J.M. Design of Complex Profile Extrusion Dies Through Numerical Modeling. *J. Non-Newton. Fluid Mech.* **2013**, *200*, 103–110.

18. Basic, H.; Demirdzic, I.; Muzaferija, M. Finite Volume Method for Simulation of Extrusion Processes. *Int. J. Numer. Methods Eng.* **2005**, *62*, 475–494.
19. Mahmoodkhani, Y.; Wells, M.A.; Parson, N.; Poole, W.J. Numerical Modelling of the Material Flow During Extrusion of Aluminum Alloys and Transverse Weld Formation. *J. Mater. Process. Technol.* **2014**, *214*, 688–700.
20. Yu, J.Q.; Zhao, G.Q.; Chen, L. Investigation of Interface Evolution, Microstructure and Mechanical Properties of Solid-State Bonding Seams in Hot Extrusion Process of Aluminum Alloy Profiles. *J. Mater. Process. Technol.* **2016**, *230*, 153–166.
21. Reggiani, B.; Donati, L. Experimental, Numerical, and Analytical Investigations on the Charge Weld Evolution in Extruded Profiles. *Int. J. Adv. Manuf. Technol.* **2018**, *99*, 1379–1387.
22. Zasadziński, J.; Libura, W.; Richert, J. Fundamentals of Advanced Aluminum Extrusion Processes. In Proceedings of the Eighth International Aluminum Extrusion Technology Seminar (ET 2004), Orlando, FL, USA 18–21 May 2004; Volume 2, pp. 391–397.
23. Saha, P.K. *Aluminum Extrusion Technology*; ASM International: Materials Park, OH, USA, 2000.
24. Klaus, A. How to Benefit from Isothermal Extrusion. In Proceedings of the Eleventh International Aluminum Extrusion Technology Seminar (ET 2016), Chicago, IL, USA, 2–6 May 2016; Volume 2, pp. 215–220.
25. Ward, T.J.; Kelly, R.M.; Jones, G.A.; Heffron, J.F. Effects of Nitrogen—Liquid and Gaseous—On Aluminum Extrusion. *JOM* **1984**, *36*, 29–33.
26. Ruppin, D.; Mueller, K. Influence of Mandrel Cooling in the Direct Extrusion of Aluminum Tubing Using Stationary or Moving Mandrels. *Alum. Düsseldorf* **1982**, *58*, 402–406.
27. Stratton, P. Raising Productivity of Aluminum Extrusion with Nitrogen. *Int. Heat Treat. Surf. Eng.* **2008**, *2*, 105–108.
28. Pelaccia, R.; Reggiani, B.; Negozio, M.; Donati, L. Liquid nitrogen in the industrial practice of hot aluminium extrusion: Experimental and numerical investigation. *Int. J. Adv. Manuf. Technol.* **2022**, *119*, 3141–3155. https://doi.org/10.1007/s00170-021-08422-3.
29. Pelaccia, R.; Negozio, M.; Di Donato, S.; Donati, L.; Reggiani, B. Recent Trends in Nitrogen Cooling Modelling of Extrusion Dies. *Key Eng. Mater.* **2024**, *987*, 11–22. https://doi.org/10.4028/p-q0ndkb.
30. Giarmas, E.; Tzimtzimis, E.; Tsongas, K.; Korlos, A.; David, C.; Tzetzis, D. Effect of Increased Extrusion Ram Speed and Liquid Nitrogen Cooling on the Mechanical Properties of 6060 Aluminum Alloy. *Metals* **2025**, *15*, 1136. https://doi.org/10.3390/met15101136.
31. Hoque, S.E.; Hovden, S.; Culic, S.; Nietsch, J.A.; Kronsteiner, J.; Horwatitsch, D. Modeling Friction in HyperXtrude™ for Hot Forward Extrusion Simulation of EN AW 6060 and EN AW 6082 Alloys. *Key Eng. Mater.* **2021**, *926*, 416–425.
32. *EN 755-9:1997*; Aluminium and Aluminium Alloys—Extruded Rod/Bar, Tube and Profiles—Part 9: Profiles, Tolerances on Dimensions and Form. CEN: Brussels, Belgium, 1997.